Volume 5, ICOLES2021 Special Issue, 2022 e-ISSN: 2667-484X

KOCAELI JOURNAL OF SCIENCE AND ENGINEERING

http://dergipark.org.tr/kojose
kojose@kocaeli.edu.tr

Printed By

Kocaeli University - Graduate School of Natural and Applied Sciences - Umuttepe Campus 41001, Kocaeli / TURKEY
Tel: +090 (262) 303 35 56 Fax: +090 (262) 303 30 33 E-mail: kojose@kocaeli.edu.tr

Kocaeli University

Kocaeli Journal of Science and Engineering

http://dergipark.org.tr/kojose

PREFACE

The 4th International Conference on Life and Engineering Sciences has been held in 23-25 September 2021 in Fenerbahçe University, İstanbul-Turkey. The aim of the conference was to bring together experts and young researchers from all over the world working in life and engineering to present their researches, exchange new ideas, discuss challenging issues, foster future collaborations and interact with each other.

The main objective of the conference was to discuss recent results in life and engineering and their applications, particularly mathematics, pyhsics, agricultural and aquatic sciences, chemistry and. We have guested many prominent experts from different countries who have presented best quality papers. The conference brought together about 150 participants from 10 countries (Algeria, Bulgaria, Croatia, Romania, Serbia, Azerbaijan, India, Iraq, Pakistan, Turkey), out of which 180 were contributing to the meeting with oral and 40 with poster presentations.

It was also a goal of the conference to promote collaborative and networking opportunities among senior scholars and graduate students in order to advance new perspectives. Additional emphasis at 4. International Conference on Life and Engineering Sciences was put on applications in related areas, as well as other science, such as natural science, economics, computer science and various engineering sciences.

The conference was devoted to several natural and applied sciences, including all fields of mathematics and variety of its applications. This issue of Kocaeli Journal of Science and Engineering contains 6 papers presented at the conference and selected by the usual editorial procedure of the journal. We would like to express our gratitude to the authors of articles published in this issue and to the referees for their kind assistance and help in evaluation of contributions. Special thanks to Kocaeli Journal of Science and Engineering for the support.

Prof.Dr. Fatma KANCA
Chair of ICOLES 2021

Kocaeli University

Kocaeli Journal of Science and Engineering

http://dergipark.org.tr/kojose

Koc. J. Sci. Eng., 5(ICOLES2021 Special Issue): (2022) 01-09 https://doi.org/10.34088/kojose.1030080

Kocaeli University

Kocaeli Journal of Science and Engineering

http://dergipark.org.tr/kojose

Solution of Parabolic Problem with Inverse Coefficient s(t) with Periodic and Integral Conditions

Irem BAGLAN [1, *]

[1] *Department of Mathematics, Kocaeli University,Kocaeli, 41300, Turkey,* ***ORCID:*** *0000-0002-1877-9791*

Article Info

Research paper

Received : *November 29, 2021*
Accepted : *January 03, 2022*

Keywords

NonlinearProblem
Inverse Problem
Integral Condition
Finite Difference Method

Abstract

In this publication, We examine the inverse parabolic parabolik with nonlocal and integral conditional. Firstly, finding the existence, uniqueness and problem of stability, numerical analysis will be done by using the finite difference method for the numerical approximation of this problem.The solution is found examining the Fourier and the iteration method and also numerical solution are given using the finite difference method and results will be mentioned in the discussion section.

1. Introduction

The inverse problems are an area of great interest to many researchers [1, 3, 5, 4]. Especially, periodic conditions are very used conditions especially in physics and engineering [2, 1, 3, 6].

$$s(t)\omega_t = \omega_{xx} + h(x,t), \tag{1}$$

$$\omega(x,0) = \vartheta(x), \quad x \in [0,\pi], \tag{2}$$

$$\omega(0,t) = \omega(\pi,t), \omega_x(0,t) = \omega_x(\pi,t), \ 0 \le t \le T, \tag{3}$$

$$L(t) = \int_0^\pi x\omega(x,t)dx, 0 \le t \le T, \tag{4}$$

where (1) is the inverse coefficient problem, (2) is the initial condition, (3) are the periodic conditions and (4) is the integral data,the domain $W := \{0 < x < \pi, 0 < t < T\}$, $\vartheta(x)$ and $f(x,t)$ are known data on $[0,\pi]$ and $\overline{W} \times (-\infty,\infty)$.

Nomenclature
$\vartheta(x)$ initial condition of x
$s(t)$ inverse coefficient
$L(t)$ energy of material
$w(x,t)$ dissipation of heat
$\omega_0(t), \omega_{ck}(t), \omega_{sk}(t)$ Fourier coefficients
$W := \{0 < x < \pi, 0 < t < T\}$ domain for x,t

* Corresponding Author: isakinc@kocaeli.edu.tr

2. Analysis of the Problem

If the conditions are met, the problem will be solved.

(S1) $L(t) \in C^1[0,T]$.

(S2) $\vartheta(x) \in C^2[0,\pi]$,

$$\vartheta(0) = \vartheta(\pi),\ \vartheta'(0) = \vartheta'(\pi),$$

$$\vartheta''(0) = \vartheta''(\pi),\ L(0) = \int_0^\pi x\vartheta(x)dx,$$

(S3)

(1) $h(x,t) \in C^3[0,\pi],\ t \in 0,T]$,

(2) $h(x,t)\big|_{x=0} = h(x,t)\big|_{x=\pi}$,

$$h_{x=0} = h_x(\pi,t)\big|_{x=\pi}, h_{xx}(0,t)\big|_{x=0} = h_{xx}(\pi,t)\big|_{x=\pi},$$

(3) $\pi\int_0^\pi h(\xi,t)d\xi - \frac{\pi}{2}\sum_{k=1}^{\infty}\frac{1}{k}\int_0^\pi h(\xi,t)\sin 2k\xi d\xi \neq 0,$

$\forall t \in 0,T]$. According to the Fourier method, we obtain

$$\omega(x,t) = \frac{\omega_0(t)}{2} + \sum_{k=1}^{\infty}[\omega_{ck}(t)\cos 2kx + \omega_{sk}(t)\sin 2kx],$$

$$\omega_0(t) = \vartheta_0 + \frac{2}{\pi}\int_0^t\int_0^\pi \frac{1}{s(\tau)} fg(\xi,\tau)d\xi d\tau,$$

$$\omega_{ck}(t) = \vartheta_{ck}e^{-(2k)^2 t} + \frac{2}{\pi}\int_0^t\int_0^\pi \frac{1}{s(\tau)}h(\xi,\tau)\cos 2k\xi e^{-(2k)^2(t-\tau)}d\xi d\tau,$$

$$\omega_{sk}(t) = \vartheta_{sk}e^{-(2k)^2 t} + \frac{2}{\pi}\int_0^t\int_0^\pi \frac{1}{s(\tau)}h(\xi,\tau)\sin 2k\xi e^{-(2k)^2(t-\tau)}d\xi d\tau.$$

$$\omega(x,t) = \frac{\vartheta_0}{2} + \frac{1}{2}\int_0^t \frac{1}{s(\tau)}h_0(\tau,u)d\tau + \sum_{k=1}^{\infty}\left[\vartheta_{ck}e^{-(2k)^2 t} + \int_0^t \frac{1}{s(\tau)}h_{ck}(\tau)e^{-(2k)^2(t-\tau)}d\tau\right]\cos 2kx \quad (5)$$

$$+ \sum_{k=1}^{\infty}\left[\vartheta_{sk}e^{-(2k)^2 t} + \int_0^t \frac{1}{s(\tau)}h_{sk}(\tau)e^{-(2k)^2(t-\tau)}d\tau\right]\sin 2kx,$$

where

$$\vartheta_0 = \frac{2}{\pi}\int_0^\pi \vartheta(x)dx,$$

$$\vartheta_{ck} = \frac{2}{\pi}\int_0^\pi \vartheta(x)\cos 2kxdx,$$

$$\vartheta_{sk} = \frac{2}{\pi}\int_0^\pi \vartheta(x)\sin 2kxdx,$$

$$h_0(t) = \frac{2}{\pi}\int_0^\pi h(x,t)dx,$$

$$h_{ck}(t) = \frac{2}{\pi}\int_0^\pi h(x,t)\cos 2kxdx,$$

$$h_{sk}(t) = \frac{2}{\pi}\int_0^\pi h(x,t)\sin 2kxdx,\ k = 1,2,3,\ldots\ .$$

According to the condition (S1)-(S3), differentiating (4), we obtain

$$\int_0^\pi x\omega_t(x,t)dx = L'(t), 0 \le t \le T. \quad (6)$$

(5) and (6)

$$\frac{1}{s(t)} = \frac{L'(t) - \pi\sum_{k=1}^{\infty}2k\left(\vartheta_{sk}e^{-(2k)^2 t} + \int_0^t \frac{1}{s(\tau)}h_{sk}(\tau)e^{-(2k)^2(t-\tau)}d\tau\right)}{\pi\int_0^\pi h(\xi,t)d\xi - \frac{\pi}{2}\sum_{k=1}^{\infty}\frac{1}{k}\int_0^\pi h(\xi,t)\sin 2k\xi d\xi} \quad (7)$$

Theorem 1. *The problem (1)-(4) has a unique solution if the conditions (S1)-(S3) are hold.*

Proof. Let's apply the absolute value to (5),we get

$$|\omega(x,t)| \le \frac{|\vartheta_0|}{2} + \left|\int_0^t \frac{1}{s(\tau)} f_0(\tau) d\tau\right|$$

$$+ \sum_{k=1}^{\infty}\left(|\vartheta_{ck}(t)| + |\vartheta_{sk}(t)|\right)$$

$$+ \sum_{k=1}^{\infty}\left|\left(\int_0^t \frac{1}{s(\tau)} h_{ck}(\tau) e^{-(2k)^2(t-\tau)} d\tau\right)\right|$$

$$+ \sum_{k=1}^{\infty}\left|\left(\int_0^t \frac{1}{s(\tau)} h_{sk}(\tau) e^{-(2k)^2(t-\tau)} d\tau\right)\right|$$

Taking Cauchy inequality of the equation,we have

$$|\omega(x,t)| \le \frac{|\vartheta_0|}{2} + \left|\left(\int_0^t d\tau\right)^{\frac{1}{2}}\left(\int_0^t\left(\int_0^{\pi} \frac{h^2(\xi,\tau)}{s^2(\tau)} d\xi\right) d\tau\right)\right|$$

$$+ \sum_{k=1}^{\infty}\left(|\varphi_{ck}(t)| + |\varphi_{sk}(t)|\right)$$

$$+ \sum_{k=1}^{\infty}\left|\left(\int_0^t e^{-2(2k)^2(t-\tau)} d\tau\right)^{\frac{1}{2}}\left(\int_0^t\left(\int_0^{\pi} \frac{h^2(\xi,\tau)}{s^2(\tau)} \cos 2k\xi d\xi\right)^{\frac{1}{2}} d\tau\right)\right|$$

$$+ \sum_{k=1}^{\infty}\left|\left(\int_0^t e^{-2(2k)^2(t-\tau)} d\tau\right)^{\frac{1}{2}}\left(\int_0^t\left(\int_0^{\pi} \frac{h^2(\xi,\tau)}{s^2(\tau)} \sin 2k\xi d\xi\right)^{\frac{1}{2}} d\tau\right)\right|$$

Applying Hölder inequality of the equation,we have

$$|\omega(x,t)| \le \frac{|\vartheta_0|}{2} + \sum_{k=1}^{\infty}\left(|\vartheta_{ck}(t)| + |\vartheta_{sk}(t)|\right)$$

$$+ \frac{\sqrt{T}}{\pi}\left(\int_0^t\left(\int_0^{\pi} \frac{h^2(\xi,\tau)}{s^2(\tau)} d\xi\right) d\tau\right)^{\frac{1}{2}}$$

$$+ \frac{1}{2\sqrt{2}\pi}\left(\sum_{k=1}^{\infty}\frac{1}{k^2}\right)^{\frac{1}{2}}\left(\sum_{k=1}^{\infty}\left(\frac{|h(x,t)|}{|s(\tau)|}\right)^2\right)^{\frac{1}{2}}$$

$$+ \frac{1}{2\sqrt{2}\pi}\left(\sum_{k=1}^{\infty}\frac{1}{k^2}\right)^{\frac{1}{2}}\left(\sum_{k=1}^{\infty}\left(\frac{|h(x,t)|}{|s(\tau)|}\right)^2\right)^{\frac{1}{2}}$$

$$|\omega(x,t)| \le \frac{|\vartheta_0|}{2} + \sum_{k=1}^{\infty}\left(|\vartheta_{ck}(t)| + |\vartheta_{sk}(t)|\right)$$

$$+ \frac{\sqrt{T}}{\pi}\frac{\|h(x,t)\|}{\|s(\tau)\|}$$

$$+ \frac{1}{4\sqrt{3}}\frac{\|h(x,t)\|}{\|s(\tau)\|} + \frac{1}{4\sqrt{3}}\frac{\|h(x,t)\|}{\|s(\tau)\|}.$$

$$|\omega(x,t)| \le \frac{|\vartheta_0|}{2} + \sum_{k=1}^{\infty}\left(|\vartheta_{ck}(t)| + |\vartheta_{sk}(t)|\right)$$

$$+ \frac{1}{4\sqrt{3}}\frac{M}{\|s(\tau)\|} + \frac{1}{4\sqrt{3}}\frac{\mathrm{M}}{\|\mathrm{s}(\tau)\|} \tag{8}$$

$\omega(x,t) \in C^{2,2}(W) \cap C^{1,0}(\overline{W})$.Since (8) is limited, this series is uniformly convergent according to the Weierstrass theorem.

$$\omega_x(x,t)=\sum_{k=1}^{\infty}(-2k)\vartheta_{ck}e^{-(2k)^2t}\sin 2kx + \sum_{k=1}^{\infty}(-2k)\sin 2kx\int_0^t\frac{1}{s(\tau)}h_{sk}(\tau)e^{-(2k)^2(t-\tau)}d\tau \quad (9)$$

$$+\sum_{k=1}^{\infty}(2k)\vartheta_{sk}e^{-(2k)^2t}\cos 2kx + \sum_{k=1}^{\infty}(2k)\cos 2kx\int_0^t\frac{1}{s(\tau)}h_{ck}(\tau)e^{-(2k)^2(t-\tau)}d\tau$$

Let's take the absolute value of both sides of (9), we have

$$|\omega_x(x,t)|\le\sum_{k=1}^{\infty}2k\left(|\vartheta_{ck}(t)|+|\vartheta_{sk}(t)|\right)$$

$$+\sum_{k=1}^{\infty}\left|(2k)\int_0^t\frac{1}{s(\tau)}h_{sk}(\tau)e^{-(2k)^2(t-\tau)}d\tau\right|$$

$$+\sum_{k=1}^{\infty}\left|(2k)\int_0^t\frac{1}{s(\tau)}h_{sk}(\tau)e^{-(2k)^2(t-\tau)}d\tau\right|$$

Applying Cauchy inequality both of side to the previous equation,we have

$$|\omega_x(x,t)|\le\sum_{k=1}^{\infty}\left(|\vartheta_{sk}'(t)|+|\vartheta_{ck}'(t)|\right)$$

$$+\sum_{k=1}^{\infty}2k\left(\left(\int_0^t e^{-2(2k)^2(t-\tau)}d\tau\right)^{\frac{1}{2}}x\left(\int_0^t\left(\int_0^{\pi}\frac{h^2(\xi,\tau)}{s^2(\tau)}\cos 2k\xi d\xi\right)^{\frac{1}{2}}d\tau\right)\right)$$

$$+\sum_{k=1}^{\infty}2k\left(\left(\int_0^t e^{-2(2k)^2(t-\tau)}d\tau\right)^{\frac{1}{2}}x\left(\int_0^t\left(\int_0^{\pi}\frac{h^2(\xi,\tau)}{s^2(\tau)}\sin 2k\xi d\xi\right)^{\frac{1}{2}}d\tau\right)\right)$$

$$|\omega_x(x,t)|\le\sum_{k=1}^{\infty}\left(|\vartheta_{sk}'(t)|+|\vartheta_{ck}'(t)|\right)$$

$$+\sum_{k=1}^{\infty}\frac{1}{\sqrt{2}}\left(\int_0^t\left(\int_0^{\pi}\frac{h^2(\xi,\tau)}{s^2(\tau)}\cos 2k\xi d\xi\right)^{\frac{1}{2}}d\tau\right)$$

$$+\sum_{k=1}^{\infty}\frac{1}{\sqrt{2}}\left(\int_0^t\left(\int_0^{\pi}\frac{h^2(\xi,\tau)}{s^2(\tau)}\sin 2k\xi d\xi\right)^{\frac{1}{2}}d\tau\right)$$

$$|\omega_x(x,t)|\le\sum_{k=1}^{\infty}\left(\left\|\vartheta_{ck}'(t)\right\|+\left\|\vartheta_{sk}'(t)\right\|\right)$$

$$+\sum_{k=1}^{\infty}\frac{1}{\sqrt{2}}\frac{M}{\|s(\tau)\|}+\sum_{k=1}^{\infty}\frac{1}{\sqrt{2}}\frac{M}{\|s(\tau)\|}$$

Since sum of x-partial derivative series($\omega_x(x,t)$) is limited, this series is uniformly convergent according to the Weierstrass theorem.

$$\omega_{xx}(x,t)=\sum_{k=1}^{\infty}(-2k)^2\vartheta_{ck}e^{-(2k)^2t}\cos 2kx + \sum_{k=1}^{\infty}(-2k)^2\int_0^t\frac{1}{s(\tau)}h_{ck}(\tau)e^{-(2k)^2(t-\tau)}\cos 2kx d\tau \quad (10)$$

$$+\sum_{k=1}^{\infty}(-2k)^2\vartheta_{sk}e^{-(2k)^2t}\sin 2kx$$

$$\sum_{k=1}^{\infty}(-2k)^2\int_0^t\frac{1}{s(\tau)}h_{sk}(\tau)e^{-(2k)^2(t-\tau)}\sin 2kxd\tau$$

Let's take the absolute value of both sides of (10),we have

$$|\omega_{xx}(x,t)|\le\sum_{k=1}^{\infty}\left(\left\|\vartheta_{ck}^{''}(t)\right\|+\left\|\vartheta_{sk}^{''}(t)\right\|\right)$$

$$+\sum_{k=1}^{\infty}(-2k)^2\left(\int_0^t e^{-2(2k)^2(t-\tau)}d\tau\right)^{\frac{1}{2}}$$

$$\left(\int_0^t\left(\int_0^{\pi}\frac{h'(\xi,\tau)}{s(\tau)}\sin 2k\xi d\xi\right)^2d\tau\right)^{\frac{1}{2}}$$

$$+\sum_{k=1}^{\infty}(-2k)^2\left(\int_0^t e^{-2(2k)^2(t-\tau)}d\tau\right)^{\frac{1}{2}}$$

$$\left(\int_0^t\left(\int_0^{\pi}\frac{h'(\xi,\tau)}{s(\tau)}\sin 2k\xi d\xi\right)^2d\tau\right)^{\frac{1}{2}}$$

$$|\omega_{xx}(x,t)|\le\sum_{k=1}^{\infty}\left(\left\|\vartheta_{ck}^{''}(t)\right\|+\left\|\vartheta_{sk}^{''}(t)\right\|\right)$$

$$+\sum_{k=1}^{\infty}\frac{1}{\sqrt{2}}\frac{M}{\|s(\tau)\|}+\sum_{k=1}^{\infty}\frac{1}{\sqrt{2}}\frac{M}{\|s(\tau)\|}$$

Since sum of xx-partial derivative series($\omega_{xx}(x,t)$) is limited, this series is uniformly convergent according to the Weierstrass theorem. So, Fourier series $\omega(x,t)$ has been the unique solution.

From the second kind of Volterra equation :

$$q(t)=F(t)+\int_0^t K(t,\tau)q(\tau)d\tau,t\varepsilon[0,T] \qquad (11)$$

where

$$q(t)=\frac{1}{s(t)},$$

$$F(t)=\frac{E^{'}(t)-\pi\sum_{k=1}^{\infty}2k\varphi_{sk}e^{-(2k)^2t}}{\pi\int_0^{\pi}h(\xi,t)d\xi-\frac{\pi}{2}\sum_{k=1}^{\infty}\frac{1}{k}\int_0^{\pi}h(\xi,t)\sin 2k\xi d\xi}, \qquad (12)$$

$$K(t,\tau)=\frac{-\pi\sum_{k=1}^{\infty}2k\left(\int_0^t\frac{1}{s(\tau)}h_{sk}(\tau)e^{-(2k)^2(t-\tau)}d\tau\right)}{\pi\int_0^{\pi}h(\xi,t)d\xi-\frac{\pi}{2}\sum_{k=1}^{\infty}\frac{1}{k}\int_0^{\pi}h(\xi,t)\sin 2k\xi d\xi} \qquad (13)$$

where

$$\pi\int_0^{\pi}h(\xi,t)d\xi-\frac{\pi}{2}\sum_{k=1}^{\infty}\frac{1}{k}\int_0^{\pi}h(\xi,t)\sin 2k\xi d\xi\neq 0 \quad ,$$

$$\forall t\varepsilon[0,T].$$

Now,let show the $F(t)$ and $K(t,\tau)$ are continuous function. Let's take the absolute value of both sides of (13),we have

$$|F(t)|\le\frac{|L'(t)|+\left|\pi\sum_{k=1}^{\infty}\frac{2k}{2k}\varphi_{ck}^{'}e^{-(2k)^2t}\right|}{\left|\pi\int_0^{\pi}h(\xi,t)d\xi-\frac{\pi}{2}\sum_{k=1}^{\infty}\frac{1}{k}\int_0^{\pi}h(\xi,t)\sin 2k\xi d\xi\right|}$$

$$\|F(t)\|\le\frac{\|L'(t)\|+\pi\sum_{k=1}^{\infty}\left\|\varphi_{ck}^{'}\right\|}{M}$$

$$|K(t,\tau)| \le \frac{\left|\pi\sum_{k=1}^{\infty}\frac{2k}{2k}\left(\int_0^t q(\tau)h_{sk}^{'}(\tau)e^{-(2k)^2(t-\tau)}d\tau\right)\right|}{\left|\pi\int_0^{\pi}h(\xi,t)d\xi-\frac{\pi}{2}\sum_{k=1}^{\infty}\frac{1}{k}\int_0^{\pi}h(\xi,t)\sin 2k\xi d\xi\right|} \tag{14}$$

$$\|K(t,\tau)\| \le \frac{\pi^2\|q(\tau)\|\|h(x,t)\|}{M}$$

According to the assumption (S1)-(S2) the $F(t)$ and the $K(t,\tau)$ (kernel) are continuous on $[0,T]$.

For the uniqueness, let's assume the opposite is the case. Let the problem has two solutions $(u,s_1),\ (v,s_2)$.

$$\omega(x,t)-v(x,t)=\frac{1}{2}\int_0^t\left(\frac{1}{s_1(t)}-\frac{1}{s_2(t)}\right)h_0(\tau)d\tau$$

$$+\sum_{k=1}^{\infty}\cos 2kx\int_0^t\left(\frac{1}{s_2(t)}-\frac{1}{s_2(t)}\right)h_{ck}(\tau)e^{-(2k)^2(t-\tau)}d\tau$$

$$+\sum_{k=1}^{\infty}\sin 2kx\int_0^t\left(\frac{1}{s_2(t)}-\frac{1}{s_2(t)}\right)h_{sk}(\tau)e^{-(2k)^2(t-\tau)}d\tau$$

$$\omega(x,t)-v(x,t)=\frac{1}{2}\int_0^t\big(q(t)-r(t)\big)h_0(\tau)d\tau$$

$$+\sum_{k=1}^{\infty}\cos 2kx\int_0^t\big(q(t)-r(t)\big)h_{ck}(\tau)e^{-(2k)^2(t-\tau)}d\tau$$

$$+\sum_{k=1}^{\infty}\sin 2kx\int_0^t\big(q(t)-r(t)\big)hf_{sk}(\tau)e^{-(2k)^2(t-\tau)}d\tau$$

where

$$q(t)=\frac{1}{s_1(t)}\ \text{and}\ r(t)=\frac{1}{s_2(t)}$$

$$|\omega-v| \le \left(\int_0^t\int_0^{\pi}h^2(x,\tau)\big(q(t)-r(t)\big)^2d\tau\right)^{\frac{1}{2}}$$

$$+\sum_{k=1}^{\infty}\cos 2kx\left(\int_0^t e^{-2(2k)^2(t-\tau)}d\tau\right)^{\frac{1}{2}}$$

$$\left(\int_0^t\int_0^{\pi}h^2(x,\tau)\big(q(t)-r(t)\big)^2\cos^2 2kxdxd\tau\right)^{\frac{1}{2}}$$

$$+\sum_{k=1}^{\infty}\sin 2kx\left(\int_0^t e^{-2(2k)^2(t-\tau)}d\tau\right)^{\frac{1}{2}}$$

$$\left(\int_0^t\int_0^{\pi}h^2(x,\tau)\big(q(t)-r(t)\big)^2\sin^2 2kxdxd\tau\right)^{\frac{1}{2}}$$

$$\|\omega-v\| \le \frac{1}{2\sqrt{3}}M\|r-q\| \tag{15}$$

$$r-q=\frac{-\pi\sum_{k=1}^{\infty}(2k)\int_0^t\int_0^{\pi}h(r-q)\sin 2kxe^{-2(2k)^2(t-\tau)}d\xi d\tau}{\pi\int_0^{\pi}hd\xi-\frac{\pi}{2}\sum_{k=1}^{\infty}\frac{1}{k}\int_0^{\pi}h\sin 2k\xi d\xi}$$

$$\|\mathrm{r(t)-q(t)}\| \le \frac{\sqrt{2}}{\left(\sqrt{2}-\pi\right)}$$

$$\|\omega - v\| \le \frac{M}{2\sqrt{3}} \frac{\sqrt{2}}{\left(\sqrt{2} - \pi\right)} \tag{16}$$

$\omega(t) = v(t)$. Hence $r(t) = q(t).$

3. Analysis of Stability of the Solution

Theorem 2. *When the assumptions (S1)-(S3) be provided, the solution of the problem(1)-(4) constantly connected the* $h, \varphi, \psi, E.$

Proof. Let $E = \{\varphi, L\}$ and $\overline{E} = \{\overline{\varphi}, \overline{L}\}$ be two sets of the data. M_i, $i = 1,2,3,4$ such that

$$\|h\|_{C^1(D)} \le M, \|\vartheta\|_{C^2[0,\pi]} \le M_1, \|\overline{\vartheta}\|_{C^2[0,\pi]} \le M_1,$$

$$\|L\|_{C^2[0,T]} \le M_2, \|\overline{L}\|_{C^2[0,T]} \le M_2.$$

Let us denote $\|E\| = (\|L\|_{C^1[0,T]} + \|\vartheta\|_{C^2[0,\pi]})$. Let (ω, q) and $(\overline{\omega}, \overline{q})$ be solutions of the problems (1)-(4).

$$\omega(x,t) - \overline{\omega}(x,t) = \frac{1}{2}\left(\vartheta_0 - \overline{\vartheta_0}\right)$$

$$+ \sum_{k=1}^{\infty} \cos 2kx \left[\left(\vartheta_{ck} - \overline{\vartheta_{ck}}\right) e^{-(2k)^2 t}\right]$$

$$+ \sum_{k=1}^{\infty} \sin 2kx \left[\left(\vartheta_{sk} - \overline{\vartheta_{sk}}\right) e^{-(2k)^2 t}\right]$$

$$+ \sum_{k=1}^{\infty} \cos 2kx \int_0^t \left(q(\tau) - \overline{q(\tau)}\right) h_{ck}(\tau) e^{-2(2k)^2 (t-\tau)} d\tau$$

$$+ \sum_{k=1}^{\infty} \cos 2kx \int_0^t \left(h_{ck}(\tau) - \overline{h_{ck}(\tau)}\right) \overline{q(\tau)} e^{-2(2k)^2 (t-\tau)} d\tau$$

$$+ \sum_{k=1}^{\infty} \sin 2kx \int_0^t \left(q(\tau) - \overline{q(\tau)}\right) h_{sk}(\tau) e^{-2(2k)^2 (t-\tau)} d\tau$$

$$+ \sum_{k=1}^{\infty} \sin 2kx \int_0^t \left(h_{sk}(\tau) - \overline{h_{sk}(\tau)}\right) \overline{q(\tau)} e^{-2(2k)^2 (t-\tau)} d\tau,$$

$$\left\|\omega - \overline{\omega}\right\| \le \frac{1}{2}\left\|\vartheta_0 - \overline{\vartheta_0}\right\|$$

$$+ \sum_{k=1}^{\infty} \left\|\vartheta_{ck} - \overline{\vartheta_{ck}}\right\| + \left\|\vartheta_{sk} - \overline{\vartheta_{sk}}\right\|$$

$$+ \left(\frac{\sqrt{T}}{\pi} + \frac{1}{4\sqrt{3}}\right) M \left\|q - \overline{q}\right\|$$

$$+ \left(\frac{\sqrt{T}}{\pi} + \frac{1}{4\sqrt{3}}\right) M \left\|h - \overline{h}\right\|$$

$$F(t) - \overline{F(t)}$$

$$= \frac{L'(t) - \pi \sum_{k=1}^{\infty} 2k e^{-(2k)^2 t} \varphi_{sk}}{\pi \int_0^{\pi} h(\xi, t) d\xi - \frac{\pi}{2} \sum_{k=1}^{\infty} \frac{1}{k} \int_0^{\pi} h(\xi, t) \sin 2k\xi d\xi}$$

$$- \frac{\overline{L'(t)} - \pi \sum_{k=1}^{\infty} 2k e^{-(2k)^2 t} \overline{\varphi_{sk}}}{\pi \int_0^{\pi} h(\xi, t) d\xi - \frac{\pi}{2} \sum_{k=1}^{\infty} \frac{1}{k} \int_0^{\pi} h(\xi, t) \sin 2k\xi d\xi}$$

Applying Cauchy, Bessel inequality and taking maksimum of $F - \overline{F}$,

$$\left\|F-\overline{F}\right\| \le \frac{1}{M}\left\|L'(t)-\overline{L'(t)}\right\|$$

$$+\frac{\pi}{M}\sum_{k=1}^{\infty}\left\|\vartheta_{sk}-\overline{\vartheta_{sk}}\right\|$$

$$K(t,\tau)-\overline{K}(t,\tau)$$

$$=\frac{\left(-\pi\sum_{k=1}^{\infty}(2k)\frac{1}{2k}\int_0^t q(\tau)h_{sk}^{'}(\tau)e^{-2(2k)^2(t-\tau)}d\tau\right)}{\pi\int_0^{\pi}h(\xi,t)d\xi-\frac{\pi}{2}\sum_{k=1}^{\infty}\frac{1}{k}\int_0^{\pi}h(\xi,t)\sin 2k\xi d\xi}$$

$$-\frac{\left(-\pi\sum_{k=1}^{\infty}(2k)\frac{1}{2k}\int_0^t \overline{q(\tau)}h_{sk}^{'}(\tau)e^{-2(2k)^2(t-\tau)}d\tau\right)}{\pi\int_0^{\pi}h(\xi,t)d\xi-\frac{\pi}{2}\sum_{k=1}^{\infty}\frac{1}{k}\int_0^{\pi}h(\xi,t)\sin 2k\xi d\xi}$$

$$\left\|K-\overline{K}\right\| \le \frac{\pi}{M}\left\|q-\overline{q}\right\|,$$

$$\left\|r-\overline{r}\right\| \le \left\|F-\overline{F}\right\|+\left\|K-\overline{K}\right\|\left\|\overline{q}\right\|+\left\|q-\overline{q}\right\|\left\|K\right\|$$

$$\left\|\omega-\overline{\omega}\right\| \le \frac{1}{2}\left\|\vartheta_0-\overline{\vartheta_0}\right\|$$

$$+\frac{\pi}{M}\sum_{k=1}^{\infty}\left\|\vartheta_{ck}-\overline{\vartheta_{ck}}\right\|+\left\|\vartheta_{sk}-\overline{\vartheta_{sk}}\right\|$$

$$+\frac{1}{M}\left\|L^{'}(t)-\overline{L^{'}(t)}\right\|$$

$$+\frac{\pi}{M}\left\|q-\overline{q}\right\|\left\|\overline{q}\right\|+\left\|q-\overline{q}\right\|\left\|K\right\|.$$

$$\left\|\vartheta-\overline{\vartheta}\right\| = \frac{1}{2}\left\|\vartheta_0-\overline{\vartheta_0}\right\|$$

$$+\frac{\pi}{M}\sum_{k=1}^{\infty}\left\|\vartheta_{ck}-\overline{\vartheta_{ck}}\right\|+\left\|\vartheta_{sk}-\overline{\vartheta_{sk}}\right\|$$

$$M_3=\max\left\{\frac{1}{2},\frac{\pi}{M}\right\}.$$

$$\left\|E-\overline{E}\right\| \le M_3\left\|\vartheta-\overline{\vartheta}\right\|+M_4\left\|L^{''}-\overline{L^{''}}\right\|$$

$$\left\|\omega-\overline{\omega}\right\| \le M_5\left\|E-\overline{E}\right\|$$

where

$$M_5=\max\left\{M_3,M_4\right\}.$$

For $E\to\overline{E}$ then $\omega\to\overline{\omega}$.

4. The Finite Difference Approximation

Using the implicit formula in (1)-(4)

$$q^j\frac{\omega_i^{j+1}-\omega_i^j}{\tau}=\frac{\omega_{i-1}^{j+1}-2\omega_i^{j+1}+\omega_{i+1}^{j+1}}{h^2}+h_i^j, \qquad (17)$$

$$\omega_i^1=\vartheta_i, \qquad (18)$$

$$\omega_0^j=\omega_N^j, \qquad (19)$$

$$\frac{\omega_1^j+\omega_{N-1}^j}{2}=\omega_N^j, \qquad (20)$$

where $1 \le i \le N$ and $0 \le j \le M$. Equal lengths $h = \frac{\pi}{M}$ and $\tau = \frac{T}{N}$,

$$q(t) = \frac{L^{'}(t) - \pi u_x(\pi, t)}{\int_0^{\pi} x f(x,t)dx}.$$

$$q^j = \frac{-\left(\left(L^{j+1} - L^j\right)/\tau\right) - \pi\left(u_N^j - u_{N-1}^j\right)/h}{(fin)^j},$$

where $L^j = L(t_j)$, $(fin)^j = \int_0^1 x f(x,t_j)dx$, $j = 0,1,\ldots,M, q^j$, u_i^j at the j-th iteration step. Finally,with the Gaussian elimination method, u_i^{j+1} and q^j can be solved.

5. Conclusions

This problem has been studied with periodic and integral conditions. This inverse problem is theoretically proved using the fourier method. Also, a finite difference scheme is made.

6. Acknowledgement

This work has been supported by Kocaeli University Scientific Research Projects Coordination Unit(ID:607). The author is thankful to the referee for his/her valuable suggestions.

Declaration of Ethical Standards

The authors of this article declare that the materials and methods used in this study do not require ethical committee permission and/or legal-special permission.

Conflict of Interest

The authors declare that they have no known competing financial interests or personal relationships that could have appeared to influence the work reported in this paper.

References

[1] Baglan I., Kanca F., Mishra V.N., 2018. Determination of an Unknown Heat Source from Integral Overdetermination Condition. Iran J Sci Technol Trans Sci, **42**(3), pp.1373–1382.

[2] Kanca F., Baglan I., 2013. Continuous dependence on data for a solution of the quasilinear parabolic equation with a periodic boundary condition. Boundary Value Problems, **28**(3), pp.55-67.

[3] Baglan I., 2015. Determination of a coefficient in a quasilinear parabolic equation with periodic boundary condition. Inverse Problems in Science and Engineering, **23**(5), pp.884–900.

[4] Cannon J.R., Lin Y., 1988. Determination of parameter p(t) in Hölder classes for some semilinear parabolic equations. Inverse Problems, **4**(3), pp.595-606.

Koc. J. Sci. Eng., 5(ICOLES2021): (2022) 10-17 https://doi.org/10.34088/kojose.1041310

Kocaeli University

Kocaeli Journal of Science and Engineering

http://dergipark.org.tr/kojose

A Study on Unsubstituted Cu(II) Phthalocyanine and Bovine Serum Albumin Bioconjugation

Çiğdem YAĞCI [1, *]

[1] *Department of Mathematics and Science Education, Kocaeli University, Kocaeli, 41001, Turkey,* ***ORCID:*** *0000-0002-7325-4197*

Article Info

Research paper

Received : *December 24, 2021*
Accepted : *February 22, 2022*

Keywords

Phthalocyanine
Bovine Serum Albumin
Sodium Dodecyl Sulphate
Aggregation
Bioconjugation

Abstract

The ground state electronic and fluorescence spectra of unsubstituted copper (II) phthalocyanine (CuPc) have been studied in the presence of bovine serum albumin (BSA) in water as a solvent. The effect of sodium dodecyl sulfate (SDS) on the solution properties of CuPc: BSA bioconjugate has also been investigated. FT-IR, UV-Vis, and fluorescence analysis have been carried to evaluate the BSA: CuPc bioconjugation. The optimum bioconjugate ratio of BSA: CuPc has been studied via UV-Vis and fluorescence spectral techniques. The collaborative effect of SDS with BSA on the aggregation of CuPc suspension has also been studied in terms of UV-Vis, fluorescence, and FT–IR analysis.

1. Introduction

As a member of aromatic macrocycle compounds based on a delocalized 18- π electron system, phthalocyanines (Pcs) exhibit very attractive chemical and physical properties in many fields [1–4]. Unique properties as high thermal stability, planarity, and symmetry encourage Pcs to use in many application fields as dyes, photodynamic therapy (PDT), semiconductors, Langmuir–Blodgett films, non-linear optics, liquid crystals, catalyst, information storage systems among others [5–11].

Besides their excellent chemical and physical properties, unique electronical and optical properties promote Pcs utilization in many other fields. Phthalocyanines exhibit characteristic Q (600 – 750 nm) ascribed to the $\pi \Rightarrow \pi^*$ transitions from the HOMO to the LUMO of the Pc^{2-} core, and B (300-400 nm) bands from the deeper $\pi \Rightarrow \pi^*$ transitions, respectively in UV-Vis spectrum. Despite all these properties, their poor solubility in water and aggregation restricts the efficiency of Pc applications [12–14].

Usually, spectroscopic techniques are utilized to understand the aggregation phenomenon of the phthalocyanines [15]. The two characteristic peak areas, Q- and B-band (Soret band) areas, dominate the UV-Vis spectra of the phthalocyanines [16]. The main characteristic Q-band peaks in the UV-Vis spectrum can be attributed to the free phthalocyanine molecules or stacked molecules within the phthalocyanine aggregates. Therefore, the degree and the nature of the aggregation in a specific solution can be deduced by examining the relevant peak intensities [17,18]. The overlapping between the π-systems of phthalocyanine molecules leads to Pc aggregates, namely dimeric or oligomeric Pc complexes, resulting in a peak at around 620–630 nm and usually a blue shift in the UV-Vis spectrum [17, 19–21].

Unsubstituted phthalocyanines are known to be poorly soluble in water and in most of the common organic solvents, strongly influencing the bioavailability, singlet oxygen production efficiency, and in vivo distribution [8,

* Corresponding Author: cyagci@kocaeli.edu.tr

22–24]. The planar nature of unsubstituted phthalocyanines with extended π electron density stimulates the aggregation property arising from the π⇒π* interactions between Pcs molecules [19, 25–29].

Having both hydrophilic and hydrophobic sites, protein molecules may be introduced to phthalocyanine molecules to diminish aggregation behavior in solution [30–32]. Serum albumins, as bovine serum albumin (BSA) and human serum albumin (HSA), are known to be the most abundant plasma protein in blood [33]. Serum albumins act as carriers for many molecules like bilirubin, fatty acids, and hemin in plasma [34,35]. Having both hydrophilic and hydrophobic sites and being easy to handle makes BSA a good candidate to investigate the effect of the BSA and the water-soluble phthalocyanine molecules interaction in photodynamic therapy (PDT) [36,37]. There have been several studies about the effect of BSA protein on PDT of Pc molecules after binding or encapsulation processes [37–41]. However, there are limited investigations in the literature on the effect of the interaction of unsubstituted phthalocyanines and BSA on the aggregation of phthalocyanines, except for the study of Larroquel, et al., in which unsubstituted zinc (II) phthalocyanine and BSA coordination are studied [42]. We have previously studied the dispersion effect of degraded cellulase enzyme on copper (II) phthalocyanine pigment [43]. Here in this work, best of our knowledge, the non-covalent binding of BSA protein to unsubstituted CuPc has been investigated for the first time in the literature. We also studied the effect of the increase of BSA concentration and the effect of SDS as a low molecular weight dispersant together with BSA on CuPc in terms of UV-Vis and fluorescence spectra of CuPc.

2. Materials and Methods

2.1 Materials

Bovine serum albumin, Cu (II) phthalocyanine, and sodium dodecyl sulfate were supplied from Sigma-Aldrich. In this work, purchased chemicals were used as received and solvents used after the purification process according to the literature [44].

2.2. Equipment

The UV-Vis spectra of the bioconjugates were recorded on A T80+ UV/VIS Spectrometer in a 1 cm pathlength quartz cell between 190-900 nm in water as a solvent. Agilent Cary Eclipse spectrophotometer was used to determine fluorescence spectra of the bioconjugate solutions via 1 cm pathlength quartz cuvettes at room temperature in water. The FT-IR spectra of the samples were studied with Shimadzu FTIR-8201 PC in the spectral range of 4000–400 cm^{-1}. KBr pellets with a 1:1000 mass ratio KBr: the sample was prepared to record the transmission. The sonication of the bioconjugate solutions was performed with QSonica, Q500 Sonicator equipped with a standard needle titanium probe (1/2 inch) submerged approximately 5 mm into the solutions. The sonication process was carried out at 20 kHz. All samples were sonicated three times for 20 seconds at 10-second intervals.

2.3. Methods

Stock BSA solutions were prepared at 2.0 mg/mL using the buffer pH 7.4, as physiological pH (adjusted with 0.2 M Na_2HPO_4). CuPc-BSA bioconjugations were prepared as follows: BSA solutions at 0.2 mg/L, 0.4 mg/L, 0.6 mg/L, 0.8 mg/L and 1.0 mg/L concentrations using the stock BSA solution and 2 mg/L (~$3.5x10^{-6}$ M) CuPc compound was added to each one. The suspensions were stirred for 20 mins with a magnetic stirrer before the homogenization using an ultrasonic apparatus. Ultrasonication was performed in a 20 s duty cycle, with 10 s of rest and 10 s generator acting.

3. Results and Discussion

3.1. FT-IR Spectroscopy

FT-IR spectrum was conducted to investigate the interaction between unsubstituted CuPc and BSA. As depicted in Figure 1, unsubstituted CuPc showed characteristic peaks at 1620 and 1592 cm^{-1} respectively attributed to the vibration bands of aromatic –C=N–, –C=C– and –C–H peaks of the phthalocyanine core ring [45]. In-plane and out plane vibration peaks arising from the bending were appeared between 725–877 cm^{-1} and 1000–1180 cm^{-1} as expected [46,47]. After the bioconjugation process, two new peaks have appeared at 2972 and 3214 cm^{-1} attributed to the -C-H vibration and to the primary amine, respectively. In addition to the bands corresponding to CuPc peaks with slight shifts, the characteristic amide I band and amide II bands of BSA at 1647 cm^{-1} and 1574 cm^{-1}, and the –NH and $–NH_2$ vibration band at around 700 cm^{-1} were also detected in the FT-IR spectrum [47–49]. It can be said from Figure 1 that BSA has been successfully adsorbed on CuPc molecules according to the FT-IR spectrum.

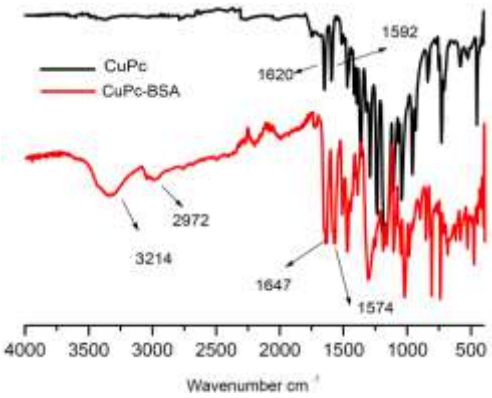

Figure 1. FT-IR spectra of CuPc and CuPc-BSA bioconjugate.

3.2. Ground State Electronic Spectroscopy

UV-Vis spectrum of CuPc is given in Figure 2. The characteristic Q-band peaks attributed to the $\pi \rightarrow \pi^*$ transitions of metallophthalocyanines can be clearly seen in the UV-Vis spectrum of CuPc at 730 and 642 nm and the Soret band at 345 nm in water [14, 51,52]. The narrow peak at 730 nm is attributed to the monomeric CuPc species and the peak at 642 nm is assigned to the aggregated CuPc molecules in water [53]. The bands at around 259 and 232 nm in Figure 2 correspond to the other aromatic sites and bis-triazine groups of the CuPc [54].

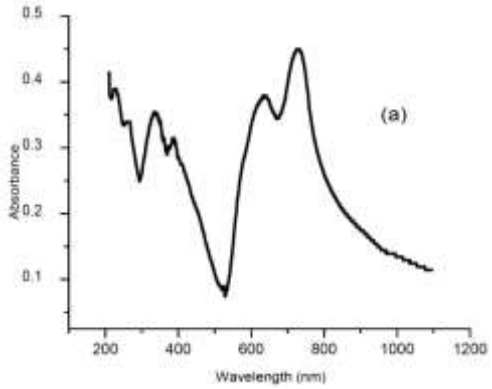

Figure 2. UV-Vis spectrum of CuPc in water (C:~3.5x10^{-6} M)

The UV-Vis spectra of CuPc after bioconjugation with BSA together with that of CuPcs' is depicted in Figure 3. The decrease in the Q- and B-bands peak intensities in the UV-Vis spectrum may be due to not only to the dilution effect as expected but also to the non-covalent interaction of CuPc and BSA molecules. Furthermore, the peak at 232 nm has been lost in Figure 3 owing to the bioconjugation [43].

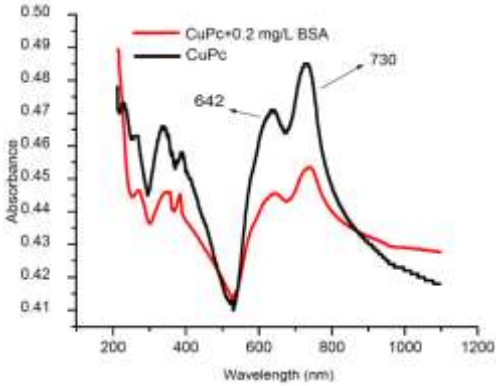

Figure 3. UV-Vis spectra of CuPc and CuPc–0.2 mg/L BSA bioconjugate

In Figure 4 and 5, the UV-Vis spectra of CuPc and various CuPc-BSA bioconjugate concentrations are given in different wavelength ranges. BSA protein exhibits two characteristic bands in the UV-Vis spectrum at around 220 nm and 280 nm due to the α-helix structure and amino acid residues, respectively [55]. According to Figure 4, there is a decrease in the Q-band intensities with the increase of BSA concentration in the bioconjugate until CuPc:0.6 mg/L BSA ratio. After the mentioned concentration ratio, an increase has been observed with the increase of BSA amount. This may be the result of the non-covalent binding of BSA molecules to unsubstituted CuPc molecules. The anionic, cationic, hydrophobic, and hydrophilic nature of proteins arises from the carboxyl, amino and methyl functional groups of the protein molecule. Hence the interactions of proteins with ligands are induced by hydrogen bonding, hydrophobic interactions, electrostatic interactions, and van der Waals forces, meanly non-covalent interactions [56,57]. The supramolecular approach can be used to explain the non-covalent interaction between phthalocyanines and protein molecules such as BSA, HSA and lipoproteins [35, 58,59]. As it is well-known that phthalocyanines are hydrophobic molecules [60,61], the interaction between CuPc and BSA may be attributed to the non-covalent binding [42,62]. At higher concentrations as 0,8 mg/L and 1,0 mg/L BSA, the Q-band absorbance was higher as can be seen in Figure 4. As the Q-band absorbance arises from the $\pi \Rightarrow \pi^*$ transitions of phthalocyanine molecules [12], this behaviour may be attributed to the lack of protein molecules that can form BSA-CuPc bioconjugate after this concentration ratio and the increase of CuPc molecules.

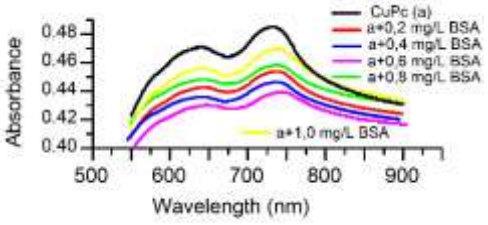

Figure 4. UV-Vis spectra of CuPc and CuPc–BSA bioconjugate at various concentrations between 500-900 nm

Moreover, similar behavior has also been detected between 220-300 nm in Figure 5. As depicted in Figure 5, the bands at around 269 and 233 nm disappeared with the addition of BSA protein as a result of bioconjugation. According to both Figure 4 and Figure 5, with 0.6 mg/L BSA addition, the optimal bioconjugate composition is achieved in our working conditions.

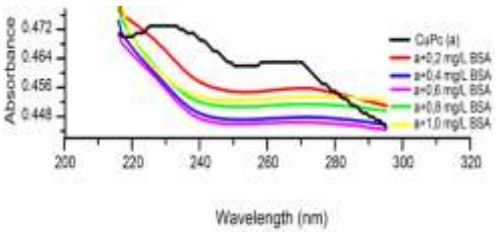

Figure 5. UV-Vis spectra of CuPc and CuPc–BSA bioconjugate at various concentrations between 200-320 nm

3.3. Fluorescence Spectroscopy

Fluorescence spectroscopy is an effective technique to evaluate the structural alterations of proteins due to the susceptible structure of aromatic amino acid, i.e. tyrosine, tryptophan, and phenylalanine, residues to the polarity of microenvironments during the excitation [63,64]. The fluorescence spectrum of CuPc and CuPc-BSA bioconjugates is given in Figure 6. The fluorescence intensity of CuPc and CuPc-BSA bioconjugates increased with the increase of BSA concentration in the bioconjugate due to the increase of aromatic amino acid species. It can be said from Figure 6 that, at CuPc-0.2 mg/L BSA bioconjugate concentration, the surface of unsubstituted CuPc has been covered by BSA molecules. However, there is no red or blue shift was observed at the maxima of the emission bands. It is known that the shifts of emission bands emerge from the changes in the hydrophobicity of the micro-environment around tryptophan residues [64]. As can be seen in Figure 6 emission maxima of the spectra showed a regular increase with the increase of BSA ratio without any shifts, suggesting that there is no change in the local dielectric environment of BSA [65].

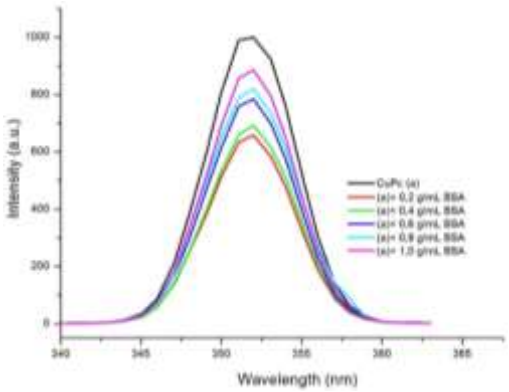

Figure 6. Fluorescence emission spectra of CuPc and CuPc-BSA bioconjugate solutions (excitation wavelength 272 nm)

3.4. SDS Effect on the Bioconjugation of CuPc and BSA Protein

The presence of an ionic detergent can affect the binding and denaturation capacity of proteins [66]. As a surfactant SDS strongly interacts with BSA and induces the proteins partial unfolding [67]. This interaction can be identified by the changes in UV-Vis and fluorescence spectra [68]. First of all, in order to understand the synergistic effect of SDS on the non-covalent binding of BSA to the CuPc molecule, UV-Vis spectra of a series of BSA: SDS mass ratios between 10:0 and 0:10 studied and the favorable mass ratio of BSA to SDS was found to be 8:2. Figure 7 shows the UV-Vis spectra of CuPc, CuPc-BSA, and CuPc-BSA-SDS bioconjugation system. As can be seen from Figure 7, the peak at 272 nm, attributed to the aromatic residues, blue-shifted 2 nm indicating the binding of SDS and BSA molecules.

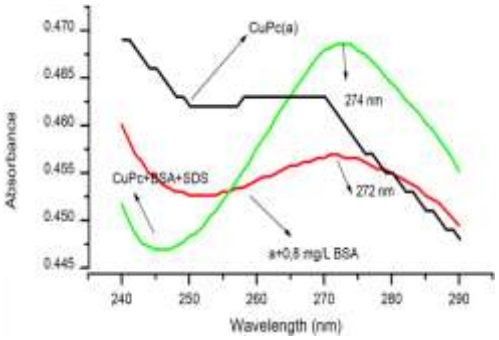

Figure 7. UV-Vis spectra of CuPc, CuPc-BSA and CuPc-BSA-SDS bioconjugation system

The fluorescence spectra of CuPc, CuPc-BSA and CuPc-BSA-SDS bioconjugation system is given in Figure 8. There was an increase in the fluorescence intensity with SDS addition as contrary to the expectation. This behavior may be the result of the increased interaction of CuPC with BSA in presence of SDS [69].

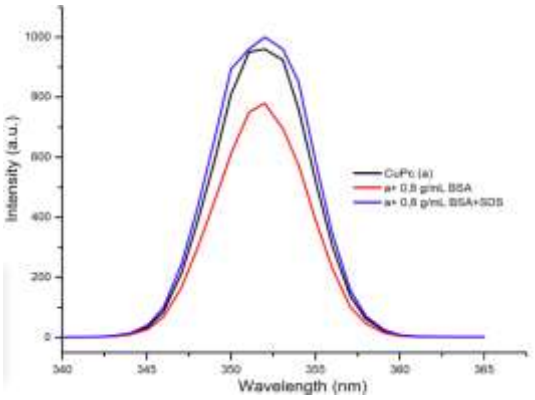

Figure 8. Fluorescence emission spectra of CuPc –CuPc–BSA and CuPc–BSA–SDS bioconjugatio n system (excitation wavelength 272 nm).

4. Conclusions

We have studied the bioconjugation of unsubstituted CuPc and BSA protein in this work. Bioconjugation was investigated via spectroscopic methods. Non-covalent interaction of CuPc and BSA was observed according to the FT-IR spectrum. The nature of the non-covalent interaction was evaluated using UV-Vis and fluorescence spectroscopy and the optimum BSA concentration for a stable bioconjugation is found to be 0.6 g/mL. SDS effect on bioconjugation of CuPc and BSA as a low molecular weight dispersant is also studied and 8:2 BSA: SDS mass ratio is found to be the most effective ratio. According to UV-Vis and fluorescence spectra SDS increased the non-covalent interaction of the CuPc-BSA bioconjugation system.

Declaration of Ethical Standards

The author(s) of this article declare that the materials and methods used in this study do not require ethical committee permission and/or legal-special permission.

Conflict of Interest

The authors declare that they have no known competing financial interests or personal relationships that could have appeared to influence the work reported in this paper.

References

[1] Hanack M., Heckmann H., Polley R., 1998. Schaumann E, editor. Houben-Weyl methods of organic chemistry. 4th ed., vol. E 9d. Phthalocyanine and Related Compounds. Stuttgart (Germany): Georg Thieme Verlag. p. 717.

[2] Claessens C. G., Hahn U., Torres T., 2008. Phthalocyanines: From Outstanding Electronic Properties to Emerging Application. Chemical Record, **8**(2), pp. 75-97.

[3] Dumoulin F., Durmuş M., Ahsen V., Nyokong T., 2010. Synthetic Pathways to Water-soluble Phthalocyanines and Close Analogs. Coordination Chemistry Reviews, **254**(23–24), pp. 2792-2847.

[4] De la Torre G., Vázquez P., Agulló-López, Torres T., 2004. Role of Structural Factors in the Nonlinear Optical Properties of Phthalocyanines and Related Compounds. Chemical Reviews, **104**(9), pp. 3723–3750.

[5] Zorlu Y., Dumoulin F., Bouchu D., Ahsen V., Lafont D., 2010. Monoglycoconjugated Water-Soluble Phthalocyanines. Design and Synthesis of Potential Selectively Targeting PDT Photosensitisers. Tetrahedron Letters, **51**(50), pp. 6615-6618.

[6] Guillaud G., Simon J., Germain J. P., 1998. Metallophthalocyanines: Gas Sensors, Resistors and Field Effect Transistors. Coordination Chemistry Reviews, **180**, pp. 1433–1484.

[7] O'Flaherty S. M., Hold S. V., Cook M. J., Torres T., Chen Y., Hanack M., Blau W. J., 2003. Molecular Engineering of Peripherally and Axially Modified Phthalocyanines for Optical Limiting and Nonlinear Optics. Advanced Materials, **15**(1), pp. 19-32.

[8] Ghani F., Kristen J., Riegler H., 2012. Solubility Properties of Unsubstituted Metal Phthalocyanines in Different Types of Solvents. Journal of Chemical and Engineering Data, **57**, pp. 439−449.

[9] Calvete M. J. F., Dini D., Flom S. R., Hanack M., Pong R. G. S., Shirk J. S., 2005. Synthesis of a Bisphthalocyanine and Its Nonlinear Optical Properties. European Journal of Organic Chemistry, **2005**(16), pp. 3499-3509.

[10] Durmuş M., Yeşilot S., Ahsen V., 2006. Separation and Mesogenic Properties of Tetraalkoxy-Substituted Phthalocyanine Isomers. New Journal of Chemistry, **30**(5), pp. 675–678.

[11] Wöhrle D., Suvorova O., Gerdes R., Bartels O., Lapok L., Baziakina N., Makarov S., Slodek A., 2004. Efficient Oxidations and Photooxidations with Molecular Oxygen Using Metal Phthalocyanines as Catalysts and Photocatalysts. Journal of Porphyrins and Phthalocyanines, **8**(08), pp. 1020–1041.

[12] Kadish K. M., Smith K. M., Guilard R. (Eds.), 2000. The Porphyrin Handbook, Vol. 15–20, Academic Press: San Diego.

[13] Kasuga K., Idehara T., Handa M., Isa K., 1992. Preparation of Unsymmetrical Phthalocyanine by Means of a Ring Expansion of Subphthalocyanine. Inorganica Chimica Acta, **196**(2), pp 127–128.

[14] Gouterman M., 1978. In The Porphyrins, Vol. 3, Dolphin D. (Ed.), Academic Press: New York.

[15] Snow A.W., 2003. The Porphyrin Handbook Phthalocyanines: Properties and Materials in Phthalocyanine Aggregation, Vol.17, K.M. Kadish, K.M. Smith, R. Guilard Eds. New York, Academic Press.

[16] Rio Y., Rodríguez-Morgade M. S., Torres T., 2008. Modulating the Electronic Properties of Porphyrinoids: A Voyage from The Violet to The Infrared Regions of The Electromagnetic Spectrum. Organic and Biomolecular Chemistry, **6**, pp. 1877–1894.

[17] Camp P. J., Jones A. C., Neely R. K., Speirs N. M., 2002. Aggregation of Copper(II) Tetrasulfonated Phthalocyanine in Aqueous Salt Solutions. Journal of Physical Chemistry A, **106**, pp. 10725– 10732.

[18] Kasha M., Rawls H. R., El-Bayoumi M. S., 1965. The Exciton Model in Molecular Spectroscopy. Pure and Applied Chemistry, **11**(3-4), pp. 371–392.

[19] Schutte W. J., Sluyters-Rehbach M., Sluyters J. H., 1993. Aggregation of an Octasubstituted Phthalocyanine in Dodecane Solution. Journal of Physical Chemistry, **97**, pp. 6069–6073.

[20] Dodsworth E. S., Lever A. B. P., Seymour P., Leznoff C. C., 1985. Intramolecular Coupling in Metal-Free Binuclear Phthalocyanines. The Journal of Physical Chemistry, **89**, pp. 5698–5705.

[21] Zelina J. P., Njue C. K, Rusling J. F., Kamau G. N., Masila M., Kibugu J., 1999. Influence of Surfactant-based Microheterogeneous Fluids on Aggregation of Copper Phthalocyanine Tetrasulfonate. Journal of Porphyrins and Phthalocyanines, **3**, pp. 188–195.

[22] De Filippis M. P., Dei D., Fantetti L., Roncucci G., 2000. Synthesis of A New Water-Soluble Octa-Cationic Phthalocyanine Derivative for PDT. Tetrahedron Letters, **41**, pp. 9143–9147.

[23] Çakır D., Çakır V, Bıyıklıoğlu Z., Durmuş M., Kantekin H., 2013. New Water-Soluble Cationic Zinc Phthalocyanines as Potential for Photodynamic Therapy of Cancer. Journal of Organometallic Chemistry, **745**, pp. 423–431.

[24] Makhseed S., Machacek M., Alfadly W., Tuhl A., Vinodh M., Simunek T., Novakova V, Kubat P., Rudolf E., Zimcik P., 2013. Water-Soluble Non-Aggregating Zinc Phthalocyanine and In Vitro Studies for Photodynamic Therapy. Chemical Communications, **49**, 11149–11151.

[25] Timoumi A., Wederni M. A., Bouguila N., Jamoussi B., AL Turkestani M. K., Chakroun R., Al-Mur B., 2021. Electrical Impedance Spectroscopy Study of Unsubstituted Palladium (II) Phthalocyanine. Synthetic Metals, **272**, pp. 116659.

[26] Heremans P., Cheyns D., Rand B. P., 2009. Strategies for Increasing the Efficiency of Heterojunction Organic Solar Cells: Material Selection and Device Architecture. Accounts of Chemical Research, **42**(11), pp. 1740–1747.

[27] George R. D., Snow A. W., Shirk J. S., Barger W. R., 1998. The Alpha Substitution Effect on Phthalocyanine Aggregation. Journal of Porphyrins Phthalocyanines, **2**, pp. 1–7.

[28] Barker C. A., Findlay K. S., Bettington S., Batsanov A. S., Perepichka I. F., Bryce M. R., Beeby A., 2006. Synthesis of New Axially-Disubstituted Silicon-Phthalocyanine Derivatives: Optical and Structural Characterization. Tetrahedron, **62**, pp. 9433–9439.

[29] Esenpınar A. A., Durmuş M., Bulut M., 2011. Photophysical, Photochemical and BSA Binding/BQ Quenching Properties of Quaternizable Coumarin Containing Water Soluble Zinc Phthalocyanine Complexes. Spectrochimica Acta Part A, **79**, pp. 608–617.

[30] Jeyachandran Y. L., Mielczarski E., Rai B., Mielczarski J. A., 2009. Quantitative and Qualitative Evaluation of Adsorption/Desorption of Bovine Serum Albumin on Hydrophilic and Hydrophobic Surfaces. Langmuir, **25**(19), pp. 11614–11620.

[31] Lang K., Mosinger J., Wagnerová D. M., 2004. Photophysical Properties of Porphyrinoid Sensitizers Non-Covalently Bound to Host Molecules; Models for Photodynamic Therapy. Coordination Chemistry Reviews, **248**(3-4), pp. 321–350.

[32] Garris J. P., Sikes C. S., 1993. Use of Polyamino Acid Analogs of Biomineral Proteins in Dispersion of Inorganic Particulates Important to Water Treatment. Colloids and Surfaces A: Physicochemical and Engineering Aspects, **80**(2-3), pp. 103–112.

[33] Mallick A., Chattopadhyay N., 2005. Photophysics in Motionally Constrained Bioenvironment: Interaction of Norharmane with Bovine Serum Albumin. Photochemistry and Photobiology, **81**(2), pp. 419–424.

[34] Curry S., 2003. Plasma Albumin as a Fatty Acid Carrier. Advances in Molecular and Cell Biology, **33**,

pp. 29–46.

[35] Varshney A., Sen P, Ahmad E., Rehan M., Subbarao N., Khan R. H., 2010. Ligand Binding Strategies of Human Serum Albumin: How Can The Cargo Be Utilized? Chirality, **22**(1), pp. 77–87.

[36] Reetz M. T., Jiao N., 2006. Copper–Phthalocyanine Conjugates of Serum Albumins as Enantioselective Catalysts in Diels–Alder Reactions. Angewandte Chemie International Edition, **45**, pp. 416–2419.

[37] Taquet J. P., Frochot C., Manneville V., Muriel B., 2007. Phthalocyanines Covalently Bound to Biomolecules for a Targeted Photodynamic Therapy. Current Medicinal Chemistry, **14**, pp. 1673–1687.

[38] Yokoi T., Hattori S., Ishii K., 2019. Encapsulation of Zinc Phthalocyanine into Bovine Serum Albumin Aggregates. Journal of Coordınatıon Chemistry, **72**(4), pp. 707–715.

[39] Borlan R., Stoia D., Gaina L., Campu A., Marc G., Perde-Schrepler M., Silion M., Maniu D., Focsan M., Astilean S., 2021. Fluorescent Phthalocyanine-Encapsulated Bovine Serum Albumin Nanoparticles: Their Deployment as Therapeutic Agents in the NIR Region. Molecules, **26**(15), pp. 4679.

[40] Barut B., Demirbaş Ü., Özel A., Kantekin H., 2017. Novel Water Soluble Morpholine Substituted Zn(II) Phthalocyanine: Synthesis, Characterization, DNA/BSA Binding, DNA Photocleavage and Topoisomerase I Inhibition. International Journal of Biological Macromolecules, **105**, pp. 499–508.

[41] Brasseur N., Langlois R., La Madeleine C., Ouellet R., van Lier J. E., 2008. Receptor-Mediated Targeting of Phthalocyanines to Macrophages Via Covalent Coupling to Native or Maleylated Bovine Serum Albumin. Photochemistry and Photobiology, **69**(3), pp. 345–352.

[42] Larroquel C., Pelegrin A., van Lier J. E., 1996. Serum Albumin as a Vehicle for Zinc Phthalocyanine: Photodynamic Activities in Solid Tumour Models. British Journal of Cancer, **74**, pp. 1886–1890.

[43] Yağcı Ç., Duman Y., 2021. Dispersant Effect of Degraded Cellulase and SDS on Copper(II Phthalocyanine Pigment. Biocatalysis and Biotransformation. **39**(4), pp. 313–321.

[44] Perrin D. D., Armarego W. L. F., 1989. Purification of Laboratory Chemicals. 2nd ed. Oxford (UK): Pergamon Press.

[45] Seoudi R., El-Bahy G.S., El Sayed Z.A., 2005. FTIR, TGA and DC Electrical Conductivity Studies of Phthalocyanine and Its Complexes. Journal of Molecular Structure, **753**(1–3), pp. 119–126.

[46] Sharp J. H., Abkowitz M., 1973. Dimeric Structure of a Copper Phthalocyanine Polymorph. The Journal of Physical Chemistry, **77**(4), pp. 477–481.

[47] Zhao Y., Wang R., Fang K., Tan Y., Chen S., Guan Y., Hao L., 2019. Investigating the Synergetic Dispersing Effect of Hydrolyzed Biomacromolecule Cellulase and SDS on CuPc Pigment. Colloids Surf B Biointerfaces, **184**, 110568.

[48] Retnakumari A., Setua S., Menon D., Ravindran P., Muhammed H., Pradeep T., Nair S., Koyakutty M., 2010. Molecular-Receptor-Specific, Non-Toxic, Near-Infrared-Emitting Au Cluster-Protein Nanoconjugates for Targeted Cancer Imaging. Nanotechnology, **21**(5), pp.055103.

[49] Ghosh D., Mondal S., Ghosh S., Saha A., 2012. Protein Conformation Driven Biomimetic Synthesis of Semiconductor Nanoparticles. Journal of Materials Chemistry, **22**(2), pp. 699–706.

[50] Della Porta V., Bramanti E., Campanella B., Tine M.R., Duce C., 2016. Conformational Analysis of Bovine Serum Albumin Adsorbed on Halloysite Nanotubes and Kaolinite: A Fourier Transform Infrared Spectroscopy Study. RSC Advances, **6**(76), 72386–72398.

[51] VanCott T. C., Rose J. L., Misener G. C., Williamson B. E., Schrimpf A. E., Boyle M. E., Schatz P. N., 1989. Magnetic Circular Dichroism and Absorption Spectrum of Zinc Phthalocyanine in an Argon Matrix between 14 700 and 74 000 cm^{-1}. Journal of Physical Chemistry, **93**, pp. 2999-3011.

[52] Cook M. J., Dunn A. J., Howe S. D., Thomson A. J., Harrison K. J., 1988. Octa-alkoxy Phthalocyanine and Naphthalocyanine derivatives: Dyes with Q-band Absorption in The Far Red or Nearinfrared. Journal of the Chemical Society, **1**(8), pp. 2453–2548.

[53] Rauf M. A., Hisaindee S., Graham J. P., Nawaz M., 2012. Solvent Effects on The Absorption and Fluorescence Spectra of Cu(II)-Phthalocyanine and DFT Calculations. Journal of Molecular Liquids, **168**, pp. 102–109.

[54] Edwards L., Gouterman M., 1970. Porphyrins XV. Vapor Absorption Spectra and Stability: Phthalocyanines. Journal of Molecular Spectroscopy, **33**, pp. 292–310.

[55] Samari F., Hemmateenejad B., Shamsipur M., Rashidi M., Samouei H., 2012. Affinity of Two Novel Five-Coordinated Anticancer Pt(II) Complexes to Human and Bovine Serum Albumins: A Spectroscopic Approach. Inorganic Chemistry, **51**(6), 3454–3464.

[56] Leckband, D., Israelachvili, J. 2001. Intermolecular Forces in Biology. Quarterly Reviews of Biophysics, **34**, pp. 105−267.

[57] Sakata S., Inoue Y., Ishihara K,. 2014. Quantitative Evaluation of Interaction Force between Functional Groups in Protein and Polymer Brush Surfaces. Langmuir, **30**, pp. 2745–2751.

[58] Kejík, Z., Kaplánek, R., B íza, T., et al., 2012. Supramolecular Approach for Target Transport of Photodynamic Anticancer Agents. Supramolecular Chemistry., **24**, pp. 106–116.

[59] Gol'dshleger N.V., Baulin V.E., Tsivadze, A.Y., 2014. Phthalocyanines in Organized Microheterogeneous Systems. Review. Protection of Metals and Physical Chemistry of Surfaces, **50**, pp. 135–172.

[60] Ali H., Langlois R., Wagner Jr., Brasseur N., Paquette B., Van Lier J., 1988. Biological Activities of Phthalocyanines-X. Syntheses and Analyses of Sulfonated Phthalocyanines. Photochemistry and Photobiology, **47**, pp. 713–719.

[61] Lo P.C., Rodriguez-Morgade M.S., Pandey R.K., Ng D.K.P., Torres T., Dumoulin F., 2020. The Unique Features and Promises of Phthalocyanines as Advanced Photosensitisers for Photodynamic Therapy of Cancer. Chemical Society, Reviews, **9**, pp. 1041–1056.

[62] Reetz M.T., Jiao N. 2006. Copper–Phthalocyanine Conjugates of Serum Albumins as Enantioselective Catalysts in Diels–Alder Reactions. Angewandte Chemie International Edition, **45**, pp. 2416–2419.

[63] Subhedar P.B., Gogate P.B., 2014. Enhancing The Activity of Cellulase Enzyme Using Ultrasonic Irradiations. Journal of Molecular Catalysis B: Enzymatic, **101**, pp. 108–114.

[64] Xue F., Xie C., Zhang Y., Qiao Z., Qiao X., Xu J., Yan S., 2012, Two New Dicopper(II) Complexes with Oxamido-bridged Ligand: Synthesis, Crystal Structures, DNA Binding/Cleavage and BSA Binding Activity. Journal of Inorganic Biochemistry, **115**, pp. 78–86.

[65] Jayabharathi J., Thanikachalam V., Perumal M.V., 2012. A Study on The Binding Interaction Between The Imidazole Derivative and Bovine Serum Albumin by Fluorescence Spectroscopy. Journal of Luminescence, **132**(3), pp. 707–712.

[66] Santos S.F., Zanette D., Fischer H., Itri R., 2003. A Systematic Study of Bovine Serum Albumin (BSA) and Sodium Dodecyl Sulfate (SDS) Interactions by Surface Tension and Small Angle X-Ray Scattering. Journal of Colloid and Interface Science, **262**, pp. 400–408.

[67] Shweitzer B., Zanette D., Itri R., 2004, Bovine Serum Albumin (BSA) Plays a Role in The Size of SDS Micelle-like Aggregates at The Saturation Binding: The Ionic Strength Effect. Journal of Colloid and Interface Science, **277**, pp. 285–291.

[68] Mondal S., Raposo M.L., Prieto G., Ghosh S., 2016. Interaction of Myoglobin with Cationic and Nonionic Surfactant in Phosphate Buffer Media. Journal of Chemical & Engineering Data, **61**(3), pp. 1221–1228.

[69] Diaz X., Abuin E.L.E., 2003. Quenching of BSA Intrinsic Fluorescence by Alkyl Pyridinium Cations: Its relationship to Surfactant-Protein Association. Journal of Photochemistry and Photobiology A: Chemistry, **155**, pp. 157–162.

Koc. J. Sci. Eng., 5(ICOLES2021): (2022) 18-24 https://doi.org/10.34088/kojose.1050267

Kocaeli University

Kocaeli Journal of Science and Engineering

http://dergipark.org.tr/kojose

Some Fractal-Fractional Integral Inequalities for Different Kinds of Convex Functions

Ebru YUKSEL [1,*]

[1] *Department of Mathematics, Ağrı İbrahim Çeçen University, Ağrı, 04100, Turkey,* ***ORCID:*** *0000-0001-7081-5924*

Article Info

Research paper

Received : *December 29, 2021*
Accepted : *February 24, 2022*

Keywords

Fractal-fractional integral operator
Hölder inequality
m-convexity
s-convexity

Abstract

The main objective of this work is to establish new upper bounds for different kinds of convex functions by using fractal-fractional integral operators with power law kernel. Furthermore, to enhance the paper, some new inequalities are obtained for product of different kinds of convex functions. The analysis used in the proofs is fairly elementary and based on the use of the well known Hölder inequality.

1. Introduction

Fractional analysis has been a field of rapid development with the definition of new integral and derivative operators in recent years, but has also closed a huge gap in terms of better identification and modeling of real-life problems. While the new fractional derivatives and integral operators continue to be examined in terms of singularity, local availability and convolution properties, another focus of researchers working in this field is to define more general operators that have applications in areas such as modeling, applied mathematics and mathematical biology.

The most frequently used derivatives of the fractional derivative in the literature are Riemann Liouville and Caputo fractional derivatives [1-3]. But as it is known, fundamental fractional derivative definitions like this include power kernel function in singular structure. Theoretically, this type of kernel functions that arise spontaneously creates difficulties in mathematical modeling for two reasons. The first of these is the computational difficulty due to singularity and the necessity of intensive numerical computations, which can often be overcome by the development of highly complex computer algorithms. The second difficulty is the inadequacy of kernel functions in the form of power functions in modeling phenomena that exhibit exponential behavior in nature.

In order to eliminate the weaknesses of fundamental derivatives, Caputo and Fabrizio replaced the kernel function of the Caputo fractional derivative with the exponential function in 2015, Atangana and Baleanu in 2016, replaced the exponential kernel function in the Caputo-Fabrizio fractional derivative with the Mittag-Leffler function, and obtained a more general definition [4,5].

These new operators, created by changing the kernel function, have been successfully used in heat transfer systems, problems such as groundwater flow in closed aquifers, wave motion on shallow water, electrical circuits, electromagnetic waves in dielectric medium.

* Corresponding Author: yuksel.ebru90@hotmail.com

In 2017, Atangana defined a new fractional operator for modeling physical events that exhibit fractal behavior in the real world [6]. This new fractional derivative and integral operator, called fractal-fractional, have been created considering the nonlocality as well as the fractal effect. Since then, many authors have applied this fractional operator in different fields based on it.

In recent years, this issue has begun to be handled with the theory of inequalities, and classical integer order integral inequalities have been generalized with fractional integral operators. Many articles, papers and postgraduate thesis studies have been made on the fractional calculus [7-21].

The fact that the inequalities obtained by the proofs can be found more general with the help of the new fractional integrals defined in recent years has prompted us to study this subject.

2. Materials and Methods

In this section, we will give a brief discussion of some important definitions and properties releated to convex functions and fractal-fractional calculus that useful for this paper.

Definition 1: [22] The function $\Psi:[u,v]\to\mathbb{R}$ is said to be convex, if we have

$$\Psi\left(\tau z_1+(1-\tau)z_2\right)\le \tau\Psi\left(z_1\right)+(1-\tau)\Psi\left(z_2\right) \tag{1}$$

for all $z_1,z_2\in[u,v]$ and $\tau\in[0,1]$.

m-convexity was defined by Toader as follows:

Definition 2: [23] The function $\Psi:[0,v]\to\mathbb{R}$, $v>0$ is said to be m-convex, where $m\in[0,1]$, if we have

$$\Psi\left(\tau z_1+m(1-\tau)z_2\right)\le \tau\Psi\left(z_1\right)+m(1-\tau)\Psi\left(z_2\right) \tag{2}$$

for all $z_1,z_2\in[0,v]$ and $\tau\in[0,1]$.

Clearly, when we take $m=1$ in this definition, then f reduces to the ordinary convex on $[0,v]$.

s-convexity introduced by Breckner as a generalization of convex functions.

Definition 3: [22] The function $\Psi:[0,\infty)\to\mathbb{R}$ is said to be s-convex in the second sense, where $s\in(0,1]$, if we have

$$\Psi\left(\tau z_1+(1-\tau)z_2\right)\le \tau^s\Psi\left(z_1\right)+(1-\tau)^s\,\Psi\left(z_2\right) \tag{3}$$

for all $z_1,z_2\in[0,\infty)$ and $\tau\in[0,1]$.

Obviously, s-convexity means just convexity when $s=1$

Recently a new concept of differential and integral operators called fractal-fractional differential and integral operators were introduced by Atangana, as the convolution of the generalized Mittag-Lefler law, exponential law and power-law with fractal derivative [6]. These operators consist of two orders, firstly the fractional-order δ then the fractal dimension ω. The purpose of the new operators is to attract nonlocal problems in nature that also display fractal behavior.

The following definitions are discussed in detail in [6].

Definition 4: [6] Suppose that $\Psi(t)$ is continuous function and fractal differentiable on an open interval (u,v) with order ω then, δ order fractal-fractional derivative of function $\Psi(t)$, power-law kernel is given by:

$${}^{FFP}_{u}D_t^{\delta,\omega}\Psi(t)=\frac{1}{\Gamma(1-\delta)}\frac{d}{dt^{\omega}}\int_u^t\Psi(s)(t-s)^{-\delta}\,ds \tag{4}$$

where $0<\omega,\delta\le 1$ and

$$\frac{d\Psi(s)}{ds^{\omega}}=\lim_{t\to s}\frac{\Psi(t)-\Psi(s)}{t^{\omega}-s^{\omega}}.$$

Definition 5: [6] Suppose that $\Psi(t)$ is continuous function and fractal differentiable on an open interval (u,v) with order ω then, δ order fractal-fractional derivative of function $\Psi(t)$, exponential decay kernel is given by:

$$\begin{aligned}{}^{FFE}_{u}D_t^{\delta,\omega}\Psi(t)&=\frac{M(\delta)}{\Gamma(1-\delta)}\\&\quad\times\frac{d}{dt^{\omega}}\int_u^t\Psi(s)\exp\left[-\frac{\delta}{1-\delta}(t-s)\right]ds\end{aligned} \tag{5}$$

where $0<\omega,\delta\le 1$ and $M(0)=M(1)=1$.

Definition 6: [6] Suppose that $\Psi(t)$ is continuous function and fractal differentiable on an open interval (u,v) with order ω then, δ order fractal-fractional derivative of function $\Psi(t)$, the generalized Mittag-Leffler kernel is given by:

$$\begin{aligned}{}^{FFM}_{u}D_t^{\delta,\omega}\Psi(t)&=\frac{AB(\delta)}{\Gamma(1-\delta)}\\&\quad\times\frac{d}{dt^{\omega}}\int_a^t\Psi(s)E_{\delta}\left[-\frac{\delta}{1-\delta}(t-s)^{\delta}\right]ds\end{aligned} \tag{6}$$

where $0<\delta,\omega\le 1$ and $AB(\delta)=1-\delta+\dfrac{\delta}{\Gamma(\delta)}$.

The fractal-fractional integral operators associated with the derivatives in Eq. (4), (5), (6) are defined as follows, respectively.

Definition 7: [6] If $\Psi(t)$ is continuous in a closed interval $[u,v]$ then the fractal integral of Ψ with order δ is defined as:

$${}^{F}_{u}J_t^{\delta}\Psi(t)=\delta\int_u^t s^{\delta-1}\Psi(s)\,ds. \tag{7}$$

Definition 8: [6] Assuming that $\Psi(t)$ is a continuous function on (u,v), then δ order fractal-fractional integral of the function $\Psi(t)$ with power-law kernel is given by:

$$ {}^{FFP}J_{u,t}^{\delta,\omega}\Psi(t)=\frac{\omega}{\Gamma(\delta)}\int_u^t (t-s)^{\delta-1}s^{\omega-1}\Psi(s)ds. \tag{8}$$

Definition 9: [6] Assuming that $\Psi(t)$ is a continuous function on (u,v), then δ order fractal-fractional integral of the function $\Psi(t)$ with an exponential decaying kernel is given by:

$$ {}^{FFE}J_{u,t}^{\delta,\omega}\Psi(t)=\frac{\delta\omega}{M(\delta)}\int_u^t s^{\delta-1}\Psi(s)ds + \frac{\omega(1-\delta)t^{\omega-1}\Psi(t)}{M(\delta)}. \tag{9}$$

Definition 10: [6] Assuming that $\Psi(t)$ is a continuous function on (u,v), then δ order fractal-fractional integral of the function $\Psi(t)$ with generalized Mittag-Leffler kernel is given by:

$$ {}^{FFM}J_{u,t}^{\delta,\omega}\Psi(t)=\frac{\delta\omega}{AB(\delta)}\int_u^t s^{\omega-1}(t-s)^{\delta-1}\Psi(s)ds + \frac{\omega(1-\delta)t^{\omega-1}\Psi(t)}{AB(\delta)}. \tag{10}$$

Remark: If the $\delta=\omega=1$, then the fractal-fractional integral operators in Eq. (8), (9) and (10) reduce to Riemann-Liouville, Caputo-Fabrizio and Atangana-Baleanu fractional integral operators respectively. Furthermore, if all fractional and fractal orders are equal to 1, the fractal-fractional integral operators reduce to the classical integral.

The purpose of this paper is to prove some fractional integral inequalities which provides the upper bounds via fractal-fractional integrals with power-law type kernel. To obtain the results, we use the different kinds of convex functions and some other features of the functions.

3. Main Results

Theorem 1: Suppose that $\Psi:[0,\infty)\to\mathbb{R}$ be a continuous function where $0\le u<t<\infty$ and $\Psi\in L_1[u,t]$. If $|\Psi|^q$ is an m-convex function, $m\in(0,1]$, then we have the following inequality for δ order fractal-fractional integral operators of the function $\Psi(t)$ with the power-law kernel:

$$ \left|\frac{\Gamma(\delta)}{(t-u)^{\delta}\omega}\,{}^{FFP}J_{u,t}^{\delta,\omega}\Psi(t)\right| \le\left(\frac{t^{1+(\omega-1)p}-u^{1+(\omega-1)p}}{(t-u)(1+(\omega-1)p)}\right)^{\frac{1}{p}} \times\left(\frac{|\Psi(u)|^q\left(q(\delta-1)+1\right)+m\left|\Psi\left(\frac{t}{m}\right)\right|^q}{\left(q(\delta-1)+1\right)\left(q(\delta-1)+2\right)}\right)^{\frac{1}{q}} \tag{11}$$

where $p^{-1}+q^{-1}=1$ and $0<\delta,\omega\le 1$.

Proof: By using definition and changing variables can be written as

$$ \frac{\Gamma(\delta)}{(t-u)^{\delta}\omega}\,{}^{FFP}J_{u,t}^{\delta,\omega}\Psi(t) =\int_0^1\tau^{\delta-1}\left(u\tau+(1-\tau)t\right)^{\omega-1}\Psi\left(u\tau+(1-\tau)t\right)d\tau. \tag{12}$$

By applying Hölder inequality, we have

$$ \left|\frac{\Gamma(\delta)}{(t-u)^{\delta}\omega}\,{}^{FFP}J_{u,t}^{\delta,\omega}\Psi(t)\right| \le\left(\int_0^1\left(u\tau+(1-\tau)t\right)^{p(\omega-1)}d\tau\right)^{\frac{1}{p}} \times\left(\int_0^1\left(\tau^{\delta-1}\right)^q\left|\Psi\left(u\tau+(1-\tau)t\right)\right|^q d\tau\right)^{\frac{1}{q}}. \tag{13}$$

By using m-convexity of $|\Psi|^q$, we obtain

$$ \left|\frac{\Gamma(\delta)}{(t-u)^{\delta}\omega}\,{}^{FFP}J_{u,t}^{\delta,\omega}\Psi(t)\right| \le\left(\int_0^1\left(u\tau+(1-\tau)t\right)^{p(\omega-1)}d\tau\right)^{\frac{1}{p}} \times\left(\int_0^1\left(\tau^{\delta-1}\right)^q\left(\tau|\Psi(u)|^q+m(1-\tau)\left|\Psi\left(\frac{t}{m}\right)\right|^q\right)d\tau\right)^{\frac{1}{q}}. \tag{14}$$

By calculating the above integrals and simplifying, the desired inequality is obtained.

Theorem 2. Suppose that $\Psi:(u,v)\subseteq[0,\infty)\to[0,\infty)$ be a continuous function and $\Psi\in L_1[u,v]$. If $|\Psi|^q$ is an s-convex function with $s\in(0,1]$, then we have the following inequality for δ order fractal-fractional integral operators of the function $\Psi(t)$ with the power-law kernel:

$$ \left|\frac{\Gamma(\delta)}{(t-u)^{\delta}\omega}\,{}^{FFP}J_{u,t}^{\delta,\omega}\Psi(t)\right| \le\left(\frac{t^{1+(\omega-1)p}-u^{1+(\omega-1)p}}{(t-u)(1+(\omega-1)p)}\right)^{\frac{1}{p}}\times\left(\frac{|\Psi(u)|^q}{2+q(\delta+1)}\right. \tag{15}$$

$$\times\left(\frac{|\Psi(u)|^q}{2+q(\delta+1)}+\frac{|\Psi(t)|^q\,\Gamma(1+(\delta-1)q)\Gamma(1+s)}{\Gamma(2+s+(\delta-1)q)}\right)^{\frac{1}{q}}$$

where $p^{-1}+q^{-1}=1$, $q>1$ and $0<\delta,\omega\le 1$.

Proof: By means of Eq. (12) and Hölder integral inequality, we can write that

$$\left|\frac{\Gamma(\delta)}{(t-u)^{\delta}\,\omega}\,{}^{FFP}J_{u,t}^{\delta,\omega}\Psi(t)\right| \le\left(\int_0^1\left(u\tau+(1-\tau)t\right)^{p(\omega-1)}d\tau\right)^{\frac{1}{p}} \times\left(\int_0^1\left(\tau^{\delta-1}\right)^q\left|\Psi\left(u\tau+(1-\tau)t\right)\right|^q d\tau\right)^{\frac{1}{q}}. \tag{16}$$

Taking into account the s-convexity of $|\Psi|^q$, we have

$$\left|\frac{\Gamma(\delta)}{(t-u)^{\delta}\,\omega}\,{}^{FFP}J_{u,t}^{\delta,\omega}\Psi(t)\right| \le\left(\int_0^1\left(u\tau+(1-\tau)t\right)^{p(\omega-1)}d\tau\right)^{\frac{1}{p}} \times\left(\int_0^1\left(\tau^{\delta-1}\right)^q\left(\tau^s|\Psi(u)|^q+(1-\tau)^s|\Psi(t)|^q\right)d\tau\right)^{\frac{1}{q}}. \tag{17}$$

By computing the above integrals and simplifying, the statement is obtained.

Corollary 1: If we take $m=1$ in Eq. (11) and $s=1$ in Eq. (16), then we get the following inequality for δ order fractal-fractional integral operators of the function $\Psi(t)$ with the power-law kernel:

$$\left|\frac{\Gamma(\delta)}{(t-u)^{\delta}\,\omega}\,{}^{FFP}J_{u,t}^{\delta,\omega}\Psi(t)\right| \le\left(\frac{t^{1+(\omega-1)p}-u^{1+(\omega-1)p}}{(t-u)(1+(\omega-1)p)}\right)^{\frac{1}{p}} \times\left(\frac{|\Psi(u)|^q\left(q(\delta-1)+1\right)+|\Psi(t)|^q}{\left(q(\delta-1)+1\right)\left(q(\delta-1)+2\right)}\right)^{\frac{1}{q}} \tag{18}$$

where $p^{-1}+q^{-1}=1$, $q>1$ and $0<\delta,\omega\le 1$.

Theorem 3. Suppose that $\Psi,\Phi:[0,\infty)\to\mathbb{R}$ be functions with $0\le u<t<\infty$ and $\Psi,\Phi,\Psi\Phi\in L_1[u,t]$. If $|\Psi|^q$ is m_1-convex and $|\Phi|^q$ is m_2-convex function on $[u,t]$ for some fixed $m_1,m_2\in(0,1]$, then we have the following inequality for δ order fractal-fractional integral operators of the function $\Psi\Phi(t)$ with the power-law kernel:

$$\left|\frac{\Gamma(\delta)}{(t-u)^{\delta}\,\omega}\,{}^{FFP}J_{u,t}^{\delta,\omega}\Psi\Phi(t)\right| \le\left(\frac{t^{1+(\omega-1)p}-u^{1+(\omega-1)p}}{(t-u)(1+(\omega-1)p)}\right)^{\frac{1}{p}} \times\left[\frac{|\Psi(u)\Phi(u)|^q}{3+(\delta-1)q} +\left(m_2\left|\Psi(u)\Phi\left(\frac{t}{m_2}\right)\right|^q+m_1\left|\Psi\left(\frac{t}{m_1}\right)\Phi(u)\right|^q\right) \times\frac{1}{(2+(\delta-1)q)(3+(\delta-1)q)} +\left|\Psi\left(\frac{t}{m_1}\right)\Phi\left(\frac{t}{m_2}\right)\right|^q \times\frac{2m_1m_2}{(1+(\delta-1)q)(2+(\delta-1)q)(3+(\delta-1)q)}\right]^{\frac{1}{q}} \tag{19}$$

where $p^{-1}+q^{-1}=1$, $q>1$ and $0<\delta,\omega\le 1$.

Proof: From the Eq. (12) and Hölder integral inequality, we get

$$\left|\frac{\Gamma(\delta)}{(t-u)^{\delta}\,\omega}\,{}^{FFP}J_{u,t}^{\delta,\omega}\Psi\Phi(t)\right| \le\left(\int_0^1\left(u\tau+(1-\tau)t\right)^{p(\omega-1)}d\tau\right)^{\frac{1}{p}} \times\left(\int_0^1\left(\tau^{\delta-1}\right)^q\left|\Psi\left(u\tau+(1-\tau)t\right)\Phi\left(u\tau+(1-\tau)t\right)\right|^q d\tau\right)^{\frac{1}{q}} \tag{20}$$

By using m-convexity of $|\Psi|^q$ and $|\Phi|^q$, we obtain

$$\left|\frac{\Gamma(\delta)}{(t-u)^{\delta}\,\omega}\,{}^{FFP}J_{u,t}^{\delta,\omega}\Psi\Phi(t)\right| \le\left(\int_0^1\left(u\tau+(1-\tau)t\right)^{p(\omega-1)}d\tau\right)^{\frac{1}{p}} \times\left(\int_0^1\left(\tau^{\delta-1}\right)^q\left|\left(\tau\Psi(u)+m_1(1-\tau)\Psi\left(\frac{t}{m_1}\right)\right)\right.\right. \left.\left.\times\left(\tau\Phi(u)+m_2(1-\tau)\Phi\left(\frac{t}{m_2}\right)\right)\right|^q d\tau\right)^{\frac{1}{q}} \tag{21}$$

$$\le \left(\int_0^1 \left(u\tau+(1-\tau)t\right)^{p(\omega-1)}\,d\tau\right)^{\frac{1}{p}} \times\left(\int_0^1 \left(\tau^{\delta-1}\right)^q \tau^2 \left|\Psi(u)\Phi(u)\right|^q d\tau + \int_0^1 \left(\tau^{\delta-1}\right)^q m_2\tau(1-\tau)\left|\Psi(u)\Phi\left(\frac{t}{m_2}\right)\right|^q d\tau + \int_0^1 \left(\tau^{\delta-1}\right)^q m_1\tau(1-\tau)\left|\Psi\left(\frac{t}{m_1}\right)\Phi(u)\right|^q d\tau + \int_0^1 \left(\tau^{\delta-1}\right)^q m_1m_2(1-\tau)^2\left|\Psi\left(\frac{t}{m_1}\right)\Phi\left(\frac{t}{m_2}\right)\right|^q d\tau\right)^{\frac{1}{q}}$$

By a simple computation, we get the desired result.

Theorem 4. Suppose that $\Psi,\Phi:(u,v)\subseteq[0,\infty)\to[0,\infty)$ be functions and Ψ, Φ, $\Psi\Phi\in L_1[u,v]$. If $|\Psi|^q$ is s_1-convex and $|\Phi|^q$ is s_2-convex function on $[u,v]$ for some fixed $s_1,s_2\in(0,1]$, then we have the following inequality for δ order fractal-fractional integral operators of the function $\Psi\Phi(t)$ with the power-law kernel:

$$\left|\frac{\Gamma(\delta)}{(t-u)^{\delta}\,\omega}\,{}^{FFP}J_{u,t}^{\delta,\omega}\Psi\Phi(t)\right| \le \left(\frac{t^{1+(\omega-1)p}-u^{1+(\omega-1)p}}{(t-u)\left(1+(\omega-1)p\right)}\right)^{\frac{1}{p}} \times\left[\frac{\left|\Psi(u)\Phi(u)\right|^q}{1+s_1+s_2+(\delta-1)q}+\frac{1}{\Gamma\left(2+s_1+s_2+(\delta-1)q\right)} \times\left(\left|\Psi(u)\Phi(t)\right|^q\left(\Gamma(1+s_2)\Gamma\left(1+s_1+(\delta-1)q\right)\right) + \left|\Psi(t)\Phi(u)\right|^q\left(\Gamma(1+s_1)\Gamma\left(1+s_2+(\delta-1)q\right)\right) + \left|\Psi(t)\Phi(t)\right|^q\left(\Gamma(1+s_1+s_2)\Gamma\left(1+(\delta-1)q\right)\right)\right)\right]^{\frac{1}{q}} \tag{22}$$

where $p^{-1}+q^{-1}=1$, $q>1$ and $0<\delta,\omega\le 1$.

Proof: By means of Eq. (12) and Hölder integral inequality, we can get

$$\left|\frac{\Gamma(\delta)}{(t-u)^{\delta}\,\omega}\,{}^{FFP}J_{u,t}^{\delta,\omega}\Psi(t)\right| \le \left(\int_0^1 \left(u\tau+(1-\tau)t\right)^{p(\omega-1)}\,d\tau\right)^{\frac{1}{p}} \times\left(\int_0^1 \left(\tau^{\delta-1}\right)^q \left|\Psi\left(u\tau+(1-\tau)t\right)\Phi\left(u\tau+(1-\tau)t\right)\right|^q d\tau\right)^{\frac{1}{q}} \tag{23}$$

Taking into account the s-convexity of $|\Psi|^q$ and $|\Phi|^q$, we have

$$\left|\frac{\Gamma(\delta)}{(t-u)^{\delta}\,\omega}\,{}^{FFP}J_{u,t}^{\delta,\omega}\Psi(t)\right| \le \left(\int_0^1 \left(u\tau+(1-\tau)t\right)^{p(\omega-1)}\,d\tau\right)^{\frac{1}{p}} \times\left(\int_0^1 \left(\tau^{\delta-1}\right)^q \left|\left(\tau^{s_1}\Psi(u)+(1-\tau)^{s_1}\Psi(t)\right) \times\left(\tau^{s_2}\Phi(u)+(1-\tau)^{s_2}\Phi(t)\right)\right|^q d\tau\right)^{\frac{1}{q}} \tag{24}$$

$$\le \left(\int_0^1 \left(u\tau+(1-\tau)t\right)^{p(\omega-1)}\,d\tau\right)^{\frac{1}{p}} \times\left(\int_0^1 \left(\tau^{\delta-1}\right)^q \tau^{s_1+s_2}\left|\Psi(u)\Phi(u)\right|^q d\tau + \int_0^1 \left(\tau^{\delta-1}\right)^q \tau^{s_1}(1-\tau)^{s_2}\left|\Psi(u)\Phi(t)\right|^q d\tau + \int_0^1 \left(\tau^{\delta-1}\right)^q \tau^{s_2}(1-\tau)^{s_1}\left|\Psi(t)\Phi(u)\right|^q d\tau + \int_0^1 \left(\tau^{\delta-1}\right)^q (1-\tau)^{s_1+s_2}\left|\Psi(t)\Phi(t)\right|^q d\tau\right)^{\frac{1}{q}}$$

By calculating the above integrals and simplifying, the desired inequality is obtained.

Corollary 2: If we take $m_1=m_2=1$ in Eq. (19) and $s_1=s_2=1$ in Eq. (22) then we get the following inequality for δ order fractal-fractional integral operators of the function $\Psi(t)$ with the power-law kernel:

$$\left|\frac{\Gamma(\delta)}{(t-u)^{\delta}\,\omega}\,{}^{FFP}J_{u,t}^{\delta,\omega}\Psi\Phi(t)\right| \le \left(\frac{t^{1+(\omega-1)p}-u^{1+(\omega-1)p}}{(t-u)\left(1+(\omega-1)p\right)}\right)^{\frac{1}{p}} \times\left[\frac{\left|\Psi(u)\Phi(u)\right|^q}{3+(\delta-1)q}+\frac{\left|\Psi(u)\Phi(t)\right|^q+\left|\Psi(t)\Phi(u)\right|^q}{\left(2+(\delta-1)q\right)\left(3+(\delta-1)q\right)} + \frac{2\left|\Psi(t)\Phi(t)\right|^q}{\left(1+(\delta-1)q\right)\left(2+(\delta-1)q\right)\left(3+(\delta-1)q\right)}\right]^{\frac{1}{q}} \tag{25}$$

4. Conclusions

In this paper, new upper bounds for different kinds of convex functions are given. To prove the main findings, fractal-fractional integral operators with power law kernel,

the properties of the functions and Hölder's inequality are used. The method adopted for generating fractional inequalities is new and simple. Using the appropriate fractional integral operators, methods can be followed to develop further results for other classes of functions. In addition, the results are useful for fractional calculus and can be an inspiration for researchers working on this subject.

Declaration of Ethical Standards

The author of this article declares that the materials and methods used in this study do not require ethical committee permission and/or legal-special permission.

Conflict of Interest

The author declares that she has no known competing financial interests or personal relationships that could have appeared to influence the work reported in this paper.

References

[1] Samko S., Kilbas A., Marichev O., 1993. Fractional Integrals and Derivatives: Theory and Applications. Gordon and Breach, Linghorne.

[2] Podlubny I., 1998. Fractional Differential Equations: An Introduction to Fractional Derivatives. Fractional Differential Equations to Methods of Their Applications vol. 198. Academic press.

[3] Lazarević M. P., Rapaić M. R., BŠekara T., 2014. Introduction to Fractional Calculus with Brief Historical Background. Advanced Topics on Applications of Fractional Calculus on Control Problems, System Stability and Modeling, WSEAS Press.

[4] Caputo M., Fabrizio M., 2015. A new definition of fractional derivative without singular kernel. Progress in Fractional Differentiation and Applications, **1**(2), pp. 73-85.

[5] Atangana A., Baleanu D., 2016. New fractional derivatives with non-local and non-singular kernel. Theory and Application to Heat Transfer Model, Thermal Science, **20**(2), pp. 763-769.

[6] Atangana A., 2017. Fractal-fractional differentiation and integration: connecting fractal calculus and fractional calculus to predict complex system. Chaos Soliton. Fract.,**102**, pp. 396-406.

[7] Anderson G. D, Vamanamurthy M. K., Vuorinen M., 2007. Generalized convexity and inequalities, J. Math. Anal. Appl, **335**, pp. 1294-1308.

[8] Kirmaci U. S., Bakula M. K, Özdemir M. E., Pecaric J., 2007. Hadamard type inequalities of s-convex functions. Applied Mathematics and Computation, **193**, pp. 26-35.

[9] Bakula M. K, Özdemir M. E., Pecaric J., 2008. Hadamard type inequalities for m-convex and (α, m)-convex functions. Journal of Inequalities in Pure and Applied Mathematics, Volume 9, Issue 4, Article 96, 12pp.

[10] Dahmani Z., 2010. On Minkowski and Hermite-Hadamard integral inequalities via fractional integration. Ann. Funct. Anal., **1**(1), pp. 51-58.

[11] Latif M. A., 2014. New Hermite-Hadamard type integral inequalities for GA-convex functions with applications. Analysis, **34**(4), pp. 379-389, doi: 10.1515/anly-2012-1235.

[12] Özdemir M. E., Latif M. A., Akdemir A. O., 2016. On some hadamard type inequalities for product of two convex functions on the co-ordinates. Turkish Journal of Science, **I**(I), pp. 41-58.

[13] Atangana A., Koca I., 2016. Chaos in a simple nonlinear system with Atangana–Baleanu derivatives with fractional order. Chaos, Solitons and Fractals, **89**, pp. 447-454.

[14] Akdemir A. O., Ekinci A., Set E., 2017. Conformable fractional integrals and related new integral inequalities. J. Nonlinear Convex Anal., **18**(4), pp. 661-674.

[15] Awan M. U., Noor M. A., Mihai M. V., Noor K. I., 2017. Conformable fractional Hermite-Hadamard inequalities via pre-invex functions. Tbilisi Math. J., **10**(4), pp. 129-141.

[16] Atangana A., 2018. Non-validity of index law in fractional calculus: a fractional differential operator with Markovian and Non-Markovian properties. Physica A: Statistical Mechanics and its Applications, **505**, pp. 688-706.

[17] Atangana A., Gomez-Aguilar J. F., 2018. Fractional derivatives with no-index law property: application to chaos and statistics. Chaos, Solitons and Fractals, **114**, pp. 516-535.

[18] Deniz E., Akdemir A. O., Yüksel E., 2019. New extensions of Chebyshev-Pòlya-Szegö type inequalities via conformable integrals. AIMS Mathematics, **4**(6), pp. 1684-1697.

[19] Akdemir A. O., Dutta H., Yüksel E., Deniz E., 2020. Inequalities for m-convex functions via ψ-Caputo fractional derivatives. Matematical Methods and

Modelling in Applied Sciences, **123**, pp. 215-224, Springer Nature Switzerland.

[20] Akdemir, A. O., Karaoglan, A., Ragusa, M. A., Set, E., 2021. Fractional integral inequalities via Atangana-Baleanu operators for convex and concave functions. J. Funct. Spaces, Vol 2021, article ID 1055434, 10 p, https://doi.org/10.1155/2021/1055434.

[21] Dlamini A., Goufo E. F. D., Khumalo M., 2021. On the Caputo-Fabrizio fractal fractional representation for Lorenz chaotic system, AIMS Mathematics, **6**(11), pp.12395-12421.

[22] Dragomir S. S., Pearce C. E. M, 2000. Selected Topics on Hermite-Hadamard Inequalities and Applications. RGMIA Monographs, Victoria University.

[23] Toader G. H., 1984. Some generalizations of the convexity. Proceedings of the Colloquium on Approximation and Optimization, Cluj-Napoca, 329-338.

Koc. J. Sci. Eng., 5(ICOLES2021): (2022) 25-31 https://doi.org/10.34088/kojose.1019125

Kocaeli University

Kocaeli Journal of Science and Engineering

http://dergipark.org.tr/kojose

SOBE: A Fraud Detection Platform in Insurance Industry

H. Onur ÖZCAN [1], İsmail ÇOLAK [2], Selin ERİMHAN [3], Vedat GÜNEŞ [4], Fatih ABUT [5,*], M. Fatih AKAY [6]

[1] *Anadolu Sigorta, Department of Business Intelligence and Analytical Solutions, Istanbul, Turkey,* ***ORCID:*** *0000-0002-2576-0212*
[2] *Anadolu Sigorta, Department of Business Intelligence and Analytical Solutions, Istanbul, Turkey,* ***ORCID:*** *0000-0002-2287-7183*
[3] *Anadolu Sigorta, Department of Business Intelligence and Analytical Solutions, Istanbul, Turkey,* ***ORCID:*** *0000-0001-5101-5235*
[4] *Anadolu Sigorta, Department of Business Intelligence and Analytical Solutions, Istanbul, Turkey,* ***ORCID:*** *0000-0002-5665-5909*
[5] *Department of Computer Engineering, Çukurova University, Adana, Turkey,* ***ORCID:*** *0000-0001-5876-4116*
[6] *Department of Computer Engineering, Çukurova University, Adana, Turkey,* ***ORCID:*** *0000-0003-0780-0679*

Article Info

Research paper

Received : November 04, 2021
Accepted : March 03, 2022

Keywords

Fraud Detection
Machine Learning
Social Network Analysis
KNIME

Abstract

Fraud detection identifies suspicious activities, false pretenses, wrongful or criminal deception intended to result in financial gain. Fraud is rare, well thought, effortful, and deceiving throughout claims. Detecting fraudulent claims is essential for the insurance industry. Therefore, most insurance companies must devote time and budget to fraud detection. Fraud detection can be divided into two categories; the main and most common type of fraud is individual fraud. Individual frauds can appear in many kinds of forms. For example, damage to an asset might be occurred before issuing a policy and be reported after. The second category is organized fraud which is much rarer and harder to detect than individual fraud. Especially motor insurance fraud is commonly attempted by organized crime rings. Counterparties involved in fraudulent claims change frequently, and changes make fraud detection difficult. According to Insurance Information and Monitoring Center findings, the fraudulent claim payment ratio is 10 to 30 %, and the detection success rate for an individual is at 1.4 to 5%. At the same time, the annual fraud cost is at 200 to 300 $ million. This study proposes a fraud detection platform called SOBE, which assists fraud departments' claim inquiry more easily and shorter than manual investigation made by employees. At its core, SOBE uses a rule engine approach. In order to support the rule engine, there is also a machine learning algorithm for fraud detection. In addition, the SNA module detects interconnected fraud counterparts among claim files. Consequently, the SOBE fraud detection platform allows Anadolu Sigorta to prevent improper payments from claiming participants. SOBE platform, the central fraud detection platform at Anadolu Sigorta, was developed in-house using different technologies and methods, including KNIME Analytics Platform, Python, graph methods, and web service methodologies.

1. Introduction

Insurance is a binding contract between the insurance company and the insurer to protect an asset against uncertain risks. In the insurance industry, fraud is one of the major problems for insurance companies. Insurance fraud may be committed by the policyholder or a third-party insurance policy claim. Fraud claim submission includes damages based on misleading or untruthful circumstances, including exaggeration of how accidents occur. On the other hand, in organized crime rings, car owners or drivers would be recruited to make false reports indicating false occurrences of vehicle accidents. These claims involve property damage or personal injuries as a result of the stated accidents [1-3].

Anadolu Sigorta offers motor and non-motor insurance policies such as health, fire, liability, marine, and car policies. Products coverages include motor policies, consisting of vehicle storage and safekeeping, towing, healthcare assistance, driver's coverage, passengers and those surrounding the vehicle, as well as legal defense expenses and minor repair services. Residential and workplace fire insurance offers services such as legal

* Corresponding Author: fabut@cu.edu.tr

consultancy and medical assistance in case of damages caused by theft, explosion, fire, internal water, vehicle impact, aircraft impact, and natural disasters such as lightning, flood, storm, landslide, and earthquake.

This study aims to develop a fraud detection platform called SOBE to detect individual and organized frauds in the insurance industry. Anadolu Sigorta was using an external program for fraud detection. We decided to develop a new fraud detection platform internally and add more essential components and capabilities for detecting frauds more efficiently. The name "SOBE" comes from the hide and seek game "You're it" in Turkish. SOBE provides significant benefits such as improvement in manual investigation of individual organized fraud cases and automation of claim files in organized fraud suspicion.

The rest of the paper is organized as follows. First, the details of the proposed SOBE platform are given. Then, the methodology and the results are presented. Finally, the paper is concluded along with future directions.

2. Related Works

Fraud detection is one of the main and hot topics in the insurance industry. It is an open issue for new R&D fields and innovation ideas. In order to understand this issue, we need to discover major problems. The main purpose is to deceive insurance companies into paying false claims [4, 5].

In related studies in the literature, some techniques have already been proposed for detecting false claims in the insurance domain. For example, Sumalatha and Prabha [6] presented a system for collecting and analyzing insurance data, including current and past insurance claims, hospital records, patient data, and offered a single platform for checking and providing suspicious claims using Logistic Regression. Sowah et al. [7] proposed Genetic Support Vector Machine (SVM)-based models using the National Health Insurance Scheme claims dataset obtained from hospitals in Ghana to detect health insurance fraud and other anomalies. Kalwihura and Logeswaren [8] introduced a data pre-processing technique, particularly a fraud behavior feature engineering approach, to prevent fraud in the auto insurance industry. Gomes et al. [9] proposed a novel deep learning methodology to gain pragmatic insights into the behavior of an insured person with the help of a new unsupervised variable importance methodology. Severino and Peng [10] evaluated fraud prediction in property insurance claims using various machine learning models based on real-world data from a major Brazilian insurance company. Rukhsar et al. [11] conducted a comparative analysis on various classification algorithms, namely SVM, Random Forest (RF), Multilayer Perceptron (MLP), Decision Tree (DT), Adaboost, K-Nearest Neighbor (KNN), Linear Regression (LR), and Naïve Bayes (NB) to detect the insurance fraud. The performance of the classifiers has been evaluated based on precision, recall, and F1-Score metrics. Despite these studies, however, the domain of organized fake claims in insurance fraud detection has not been sufficiently investigated in the literature.

Rulesets in fraud detection systems are widely used. As mentioned in [12], rule generation and selection methodologies give a solid idea of how to effectively deal with fraud detection across industry boundaries, including applications in insurance fraud, credit card fraud, healthcare fraud, telecommunications fraud, and more. A genetic algorithm is another method of artificial intelligence that was designed so that each individual represents a possible behavioral model. This approach increases the detection rate and decreases the low false alarm rate [13].

If an applicant files a claim, the insurance company will perform various checks to flag the claim as suspicious or nonsuspicious. When the claim is considered suspicious, the insurance firm will first decide whether it's worthwhile to pursue the investigation. Obviously, this will also depend on the amount of the claim, such that small amounts of claims are most likely not further considered, even if they are fraudulent. When the claim is considered worthwhile to investigate, the firm might start a legal procedure resulting in a court judgment and/or legal settlement flagging the claim as fraudulent or not. Also, this procedure is not 100 percent error-proof, and thus nonfraudulent claims might end up being flagged as fraudulent or vice versa [14].

Our study aims to internalize traditional fraud detection processes in auto and nonauto branches. In addition to traditional methods like fraud detection rulesets and ML prediction, new features like text processing from expert reports, network analysis from organized fraud detection, and run-time anomaly detection alerts are additional key features.

3. Proposed "SOBE" Platform

The lifecycle of the SOBE project consists of six stages. The first stage is to get the data from the Anadolu Sigorta source system. We transformed, organized, and stabilized the data for the next stages via web service configuration. We used REST API methodology and KNIME Analytics Platform transformation capabilities for the stage. The input data includes 567 and 543 parameters for motor and non-motor claim files, respectively, which contain both categorical and quantitative parameters. We followed the general steps of Exploratory Data Analysis techniques. We employed data transfigurations such as data formatting, constant column filtering, correlation filtering, missing value, and outlier handling methods for different

variables. Also, we used one hot encoding method to transform some categorical variables into numerical ones. For outlier handling, we used Inter Quantile Range methodology. For normalizing the data, we used both min-max scaling and Z-score normalization according to the data. Also, we generated new variables using the existing parameters to group the data into meaningful categorical variables. We used the cardinality of the historical data, K-means claustration, and Silhouette Coefficient to determine the groups. We applied the weight of evidence methodology to generalize the quantitative parameters. We utilized forward and backward elimination for feature selection, and for dimension reduction, we preferred PCA techniques.

The second stage is the Social Network Analysis (SNA). This stage is running only for motor claims. We utilized graph theory to develop the capability to reveal claim participant/claimant relationships with insurance blacklists or assets on created claim files. We mainly employed this stage to discover organized crime relations on our full set of data by adding external data sources. We selected the participant's Turkish Identification Number as the main entity for constructing the network according to the regulations legally to protect the anonymity of the participants. We characterized networked structures in terms of nodes (i.e., individual actors, people within the network) and the ties, edges, or links (relationships or interactions and assets) that connect them. Finally, we used the shortest path algorithm to determine the direct path between the blacklisted people and the participants of the claim files.

The third stage is our machine learning model to predict the fraud potential for the claim file itself. Again, this stage is running only for motor claims. We employed two different machine learning algorithms, including RF and MLP. We examined the two model outputs and decided to continue with the RF algorithm. Currently, RF has enough accuracy and speed to predict the fraud potential of the claim file.

The fourth stage is the claim search history. We collect the history of a claim's participants and subjected asset history at this stage. In addition to these, we also search if any aspect of the claim, participant, or the asset, ever occurred in another fraud case. The fifth stage is the rule engine stage which includes business rules determined by our claims departments according to their experience in the field. We have 600 rules run for every claim. Every rule has a score given by our claims department. These are some of the examples of the mentioned rules: "Claim city is different from customer city", "Claim party has other policies in force for the same vehicle with the same or other insurance company at the time of the event", "There is more than five days between the date of the claim occurred and the date of the report". After all the stages, we calculate and send a file fraud score to our claim platform within 5 to 10 seconds.

The SOBE fraud detection lifecycle starts with a web service request from Claim Management System (CMS). As soon as the claim file is reported, CMS automatically sends fraud scoring requests at certain checkpoints. This request is sent to the KNIME server via Rest API and includes individual claim file details. KNIME server architecture accepts only JSON files on REST calls, so the requests and SOBE responses are sent in JSON format. To prevent load latency, a certain number of jobs are pooled on the KNIME server. So, when a request is sent from the CMS, the SOBE workflow is immediately executed in the server. Figure 1 illustrates external data integration via web services.

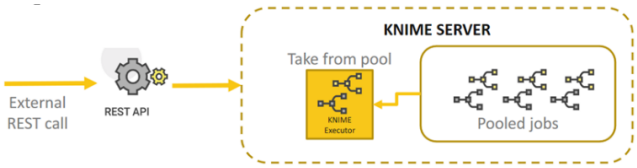

Figure 1. External data integration via web services

Figure 2 represents the overview of a SOBE workflow. The steps can be explained as follows:

1. Data transformation, standardization, and normalization step: Webservice request contains data from the CMS. Before using this input in the rule engine and ML prediction steps, several data transformations are applied.

2. SNA + Blacklist: The participants of the claim file (mainly policyholders) are searched for any existing connections in an organized fraud scheme. SNA results include Anadolu Sigorta and Insurance Information and Monitoring Center data. In this step, the company blacklist is also used to label participants of the claim file.

3. Machine learning model: The RF-based model for auto claims classifies the claim as fraudulent or not.

4. History search: To check recurring claims of a certain participant in the claim file, a history search is executed in this step (e.g., number of rejected claims for the claimant for motor). The results are used in the rule engine step.

5. Rule engine: The claim file is scored according to active rules. Also, ML model predictions, SNA, and blacklist results are taken into consideration in scoring.

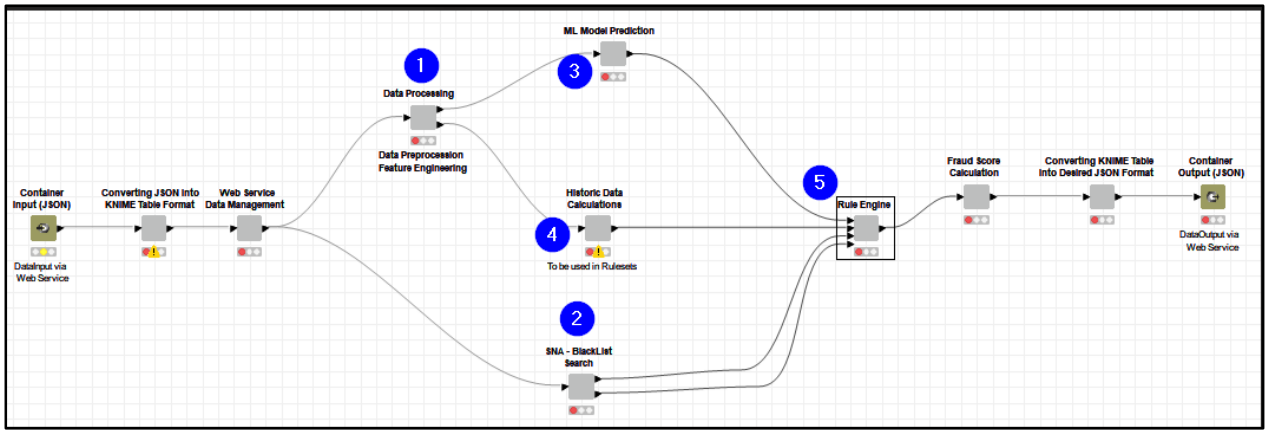

Figure 2. Overview of a "SOBE" workflow

4. Methodology

In insurance, a claim file has several phases called "touchpoint". Those phases contain several steps like file opening, expert opinion, file status changes. At the very beginning, the ML model tries to decide if the claim file has a fraud suspicious or not.

Since the fraud case is a good example of an imbalanced dataset, cleaning and selecting the right data to balance the target variable with the business side's opinions is crucial for modeling. After applying Exploratory Data Analysis (EDA) steps and balancing data as much as possible (i.e., 7% fraud cases in target variable), RF-based and MLP-based models have been created. With hyper-parameter optimizations, each model has been implemented on validation data that was not used during the training phase. For the RF-based model, we generated 100 trees using Gini Index and Information Gain Ratio and 100 different stratified sampled data partitioned via loops. In the MLP-based model build, epsilon is kept in 1e-8, and the number of maximum iterations is limited by 120 with an initial learning rate of 0.001. ReLU is used as the hidden layer activation function. In addition, several numbers of hidden layers ranging from one to six and different numbers of neurons varying between 8 and 35 have been tested during the MLP-based model training.

We evaluated the performance of the two models by calculating the precision, recall, F-Measure, and accuracy values, as defined in Eqs. (1) through (4), respectively, where tp is the ratio of true positives, tn is true negatives, fn shows false negatives, and fp represents false positives. In order to eliminate the overfitting danger while building the model, the 10-fold cross-validation method has been used to evaluate the generalization error of the models.

$$Precision = \frac{tp}{tp+fp} \tag{1}$$

$$Recall = \frac{tp}{tp+fn} \tag{2}$$

$$F - Measure = \frac{2*Precision*Recall}{Precision + Recall} \tag{3}$$

$$Accuracy = \frac{tp+tn}{tp++tn+fp+fn} \tag{4}$$

Organized fraud detection is a different discipline that uses other techniques than traditional ML methods. Using graph theory is one of the solutions to that problem. In that phase of fraud detection, the aim is to detect the relationships of blacklisted persons with claim file participants in a huge network (e.g., a network consisting of 8 million nodes and 12 million connections). The network has been constructed not only with Anadolu Sigorta claim data but with external data sources like accident report files (KKT-Kaza Tespit Tutanağı) and Insurance Information and Monitoring Center (SBM-Sigorta Bilgi Merkezi) insurers data. Network connections have been constructed basically with vehicle chassis numbers and participants' identification numbers.

After the network has been established, blacklisted people have been labeled within the network to see the relationships with other participants. In Figure 3, the red-colored node is a blacklisted person, and the green-colored node is the participant being investigated for an organized fraud scenario.

Once the connections have been established, the next challenge is to detect the relationships in terms of closeness, strengths, and organized crime suspicious. The main solution to that problem is finding the shortest path between participants. When the shortest path algorithm has been applied to the network, the shortest path between two participants can be revealed easily. Within daily incoming

claim files, first and second-degree connections of participants with blacklisted people, using the same chassis number among participants and their degrees, and a participant's number of connections are investigated and scored with respect to importance to support the fraud detection system.

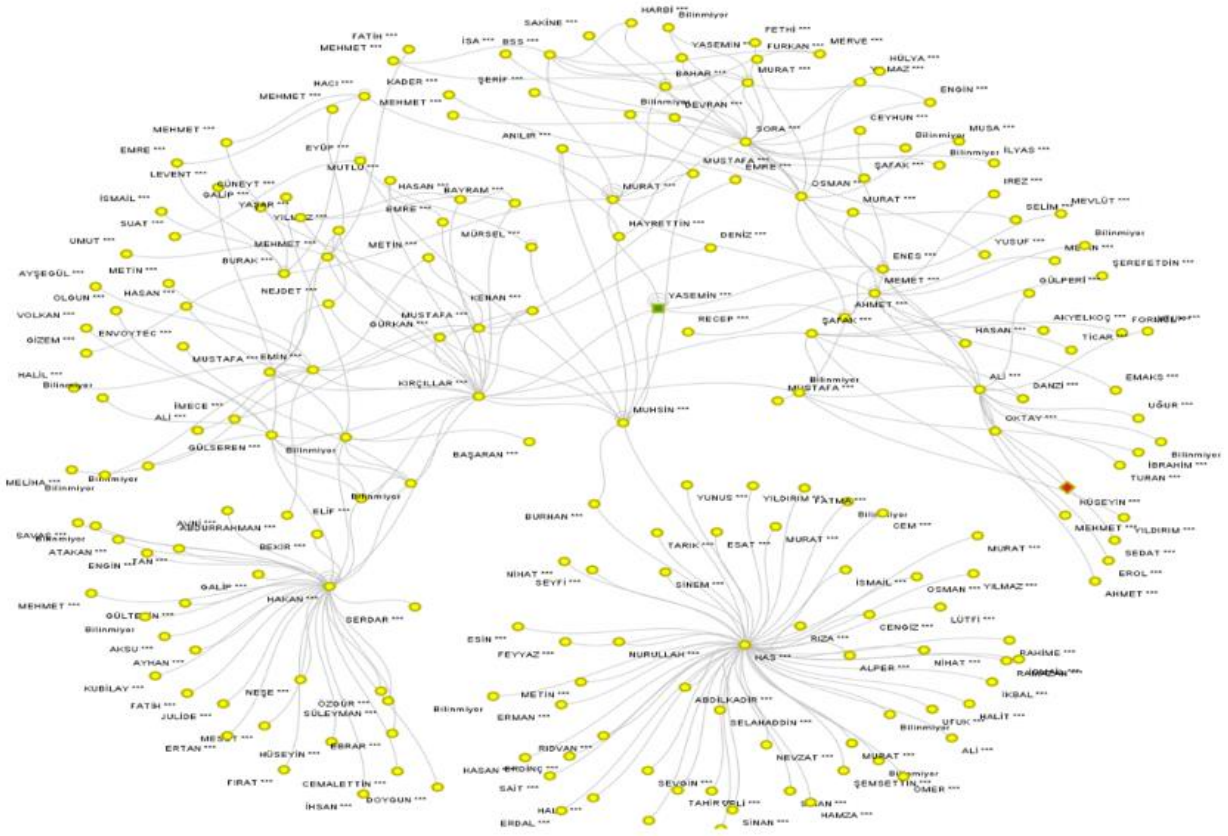

(a)

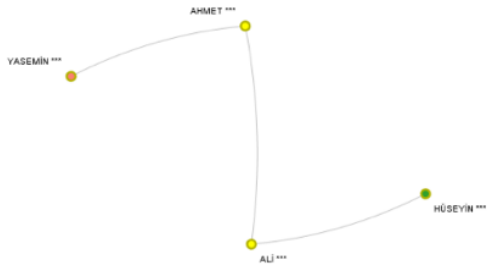

(b)

Figure 3. The output view of the SNA module

5. Results

The performance of the models has been confirmed by applying the cross-validation step for model generalization and calculating the precision and recall values. The priority is to keep recall as high as possible while also keeping precision at an acceptable rate. Considering this priority, the RF-based model produced precision, recall, F-measure, and accuracy values of 0.274, 0.374, 0.316, and 95.83%, respectively, whereas the MLP-based model yielded precision, recall, F-measure, and accuracy values of 0.537, 0.298, 0.383, and 97.51% respectively.

SOBE platform has replaced the purchased fraud application, and it is the central application used by the Anadolu Sigorta Claim department. The platform handles over 2500 claim cases daily and predicts the probability of fraud for each file in less than 10 seconds. Integrated module

architecture makes the platform simple and manageable for both business and technology-wise.

All the fraud detection platform stages, the rule set determination, score prediction with a machine learning algorithm, and SNA results give the fraud score of the claim record. Our operational process is triggered based on this score, and further steps run until the file is closed.

The process of developing the SOBE platform has resulted in various gains. The benefits of the application can be outlined as follows:

- We tailor our own fraud platform from the beginning of the process: data preparation, data enrichment, quality study, rule definitions, and SNA platform integrated file investigation. This is the first platform ever developed in the insurance sector.
- The purchased platform has been eliminated, and there is no subscription/maintenance cost anymore.
- Our claims department can determine faster for the claim investigation on a suspicious file.
- The system is in-house, so implementation, maintenance, and development of the platform can be done easier.
- Platform health check process will be done internally, and there is no dependency on a vendor company.

The SOBE platform went live in Sept 2021, and its efficiency has been compared to our previous platform based on quarter 4 (Q4) of the years 2020 and 2021. Table 1 shows the comparison results.

Table 1. Comparing the SOBE and our previous platforms

	Previous Platform	**SOBE Platform**
Total savings	2020 Q4: 8.3 million TL	2021 Q4: 12.8 million TL
Fraud detection ratio	2020 Q4: 8.36%	2021 Q4: 12.69%
SNA output	n/a	5 organized fraud rings
SNA savings	n/a	2.2 million TL

6. Conclusion and Future Work

This study proposed SOBE, a fraud detection platform that allows Anadolu Sigorta to prevent improper payments from claiming participants. SOBE improves manual investigation of individual organized fraud cases and automates processing claim files in organized fraud suspicion. We managed to perform a detailed analysis and determine if a claim has fraud risk or not throughout a claim lifecycle.

In the following steps, the study can be extended in multiple ways. SOBE can also be extended to consider anomaly detection scenarios. Machine learning algorithms can be developed for non-motor claims. The collection of historical data could be expanded by adding external data sources. From all kinds of reports in the CMS, keyword extraction and expert fraud opinions can be extracted from the reports. Also, additional ML models could be implemented in critical touchpoints to detect fraud cases more precisely with the enriched data.

Declaration of Ethical Standards

The authors of this article declare that the materials and methods used in this study do not require ethical committee permission and/or legal-special permission.

Conflict of Interest

The authors declare that they have no known competing financial interests or personal relationships that could have appeared to influence the work reported in this paper.

References

[1] Ribeiro R., Silva B., Pimenta C., & Poeschl G., 2020. Why do consumers perpetrate fraudulent behaviors in insurance?. Crime, Law and Social Change, **73**(3), pp. 249-273.

[2] Abdallah A., Maarof M. A., & Zainal A., 2016. Fraud detection system: A survey. Journal of Network and Computer Applications, **68**, pp. 90-113.

[3] Hargreaves C. A., & Singhania V., 2015. Analytics for Insurance Fraud Detection: An Empirical Study. American Journal of Mobile Systems, Applications and Services, **1**(3), pp. 223-232.

[4] Liu X., Yang J. B., Xu D. L., 2020. Fraud detection in automobile insurance claims: a statistical review. In: Developments of Artificial Intelligence Technologies in Computation and Robotics: Proceedings of the 14th International FLINS Conference, pp. 1003-1012.

[5] Patil K. S., Godbole A., 2018. A survey on machine learning techniques for insurance fraud prediction. Helix, **8**(6), pp. 4358-4363.

[6] Sumalatha M. R., Prabha M., 2019. Mediclaim fraud detection and management using predictive analytics. In: Proc. of Intl. Conference on Computational Intelligence and Knowledge Economy, pp. 517-522.

[7] Sowah R. A., Kuuboore M., Ofoli A., Kwofie S., Asiedu L., Koumadi K. M., Apeadu K. O., 2019. Decision support system for fraud detection in health insurance claims using genetic support vector machines. Journal of Engineering, Article ID 1432597.

[8] Kalwihura J. S., Logeswaran R., 2020. Auto-insurance fraud detection: a behavioral feature engineering approach. Journal of critical reviews, **7**(3), pp. 125-129.

[9] Gomes C., Jin Z., Yang H., 2021. Insurance fraud detection with unsupervised deep learning. Journal of Risk and Insurance, **88**, pp. 591–624.

[10] Severino M. K., & Peng Y., 2021. Machine learning algorithms for fraud prediction in property insurance: Empirical evidence using real-world microdata. Machine Learning with Applications, **5**, 100074.

[11] Rukhsar L., Bangyal W. H., Nisar K., & Nisar S., 2022. Prediction of insurance fraud detection using machine learning algorithms. Mehran University Research Journal of Engineering & Technology, **41**(1), pp. 33-40.

[12] Baesens B., Van Vlasselaer V., Verbeke W., 2015. Fraud Analytics Using Descriptive, Predictive, and Social Network Techniques. John Wiley & Sons, Inc

[13] Katoch S., Chauhan S.S. & Kumar V., 2021. A review on genetic algorithm: past, present, and future. Multimedia Tools and Applications, **80**, pp. 8091-8126.

[14] Dokas P., Ertoz L., Kumar V., Lazarevic A., Srivastava J., & Tan P. N., 2002. Data mining for network intrusion detection. In: Proc. of NSF Workshop on Next Generation Data Mining (pp. 21-30).

Koc. J. Sci. Eng., 5(ICOLES2021): (2022) 32-37 https://doi.org/10.34088/kojose.1019277

Kocaeli University

Kocaeli Journal of Science and Engineering

http://dergipark.org.tr/kojose

Brand Propensity Prediction with Click-Through Rate as a Target

Alptekin UZEL [1], Kaan PEKEL [2], Fatih ABUT [3,*], M. Fatih AKAY [4]

[1] *Trendyol, Istanbul, Turkey,* ***ORCID:*** *0000-0002-1563-743X*
[2] *Trendyol, Istanbul, Turkey,* ***ORCID:*** *0000-0001-5482-2999*
[3] *Department of Computer Engineering, Çukurova University, Adana, Turkey,* ***ORCID:*** *0000-0001-5876-4116*
[4] *Department of Computer Engineering, Çukurova University, Adana, Turkey,* ***ORCID:*** *0000-0003-0780-0679*

Article Info

Research paper

Received : November 04, 2021
Accepted : May 19, 2022

Keywords

Logistic Regression
Ensemble Model
Brand Propensity
Prediction

Abstract

Personalizing the e-commerce experience is vital since there are enormous amounts of products to offer customers. Each day new products are introduced into the ecosystem, and customer purchase behavior is dynamic as well. This mapping between products and customers needs to be optimized. E-commerce platforms try to funnel those products by a variety of methods like user clustering and product propensity analysis. The brand propensity metric is one of those key features for personalizing products offered to the customer. Once the brand propensity is calculated, it can be used to cluster customers or list products within the same brand. Since customers periodically interact with different products, these interactions (e.g., product visit, favorite, basket, search, and order) are aggregated to predict the next actions of the corresponding customer. Typically, the next action might be an order action or click. In this study, we develop Logistic Regression (LR) models to investigate the effect of the target variable on calculating brand propensity. For comparison purposes, models based on Decision Tree (DT), Random Forest (RF), and XGBoost (XGB) have also been developed. The target variable to be evaluated for the brand propensity model has been set to both order probability and click probability. The "Top N accuracy" metric has been used to evaluate the performance of the models. As the study's outcome, click as a target variable has been revealed to be more beneficial since it also shows that customers are more likely to explore what is inside that brand. In addition, the LR-based propensity models exhibit the best average performance for both Top 3 and Top 5 accuracies among the machine learning methods.

1. Introduction

One of the key problems in e-commerce is the mapping of products and customers: which product subset should be associated with which user cluster? In the personalization aspect, these clusters are the customers themselves. So, for each person, personalized product recommendations can be created. Then comes the next problem: the dimension of those product recommendations. The most common dimensions are brand, category, and price. All those factors can define user behavior such that specific sets of products can be recommended [1–3].

Services of e-commerce platforms reach the customer via applications and web pages. So, product recommendations have user experience (UX) components. In applications, those components are called widgets. Each widget can cover different dimensions of the product recommendation. Some can be associated with categories, whereas others with brands or prices.

This study proposes Logistic Regression (LR) models to investigate the effect of changing the target variable on brand propensity prediction. For comparison purposes, models based on Decision Tree (DT), Random Forest (RF), and XGBoost (XGB) have also been developed. The target variable to be evaluated for the brand propensity model has been set to both order and click probabilities. Personalized brands are sorted and recommended to the customers in a

* Corresponding Author: fabut@cu.edu.tr

brand slider widget. In this context, it is a ranking and sorting problem. Product and customer data of the e-commerce site Trendyol is used in this problem. Each customer interacts with different products through the application. These interactions (e.g., product visit, favorite, basket, search, and order) constitute the signals/features for the machine learning model to interpret. They are aggregated by brand and used to predict customers' actions on that brand. The problem also has a time domain, so it is also related to forecasting. The action features are aggregated as time-lagged features (i.e., one day, seven days, two weeks, etc.) to tune the effects of those signals in the expected actions.

The rest of the paper is organized as follows. First, the related works are summarized. Then, the details of the developed models and the methodology are introduced to predict the brand propensity for each customer. Next, the results are presented. Finally, the paper is concluded along with possible future works.

2. Related Works

The next purchase prediction of the customers in an e-commerce platform based on the customer and product interaction data has been investigated for a relatively long time. In recent years, deep learning models and ensemble methods are also adapted to the problem. The following studies helped to shape the idea presented in this paper.

Zhang [4] compared several LR and RF metrics for predicting customer propensity in an e-commerce platform. Valecha et al. [5] discussed consumer behavior by applying a predictive model to a dataset in Kaggle. Szabó and Geng [6] used a novel approach to create a sequence of numbers to represent customer behavior and then applied deep learning methods to use this as a feature to predict purchases. Liu and Li [7] used similar data to predict purchase behavior and applied the Support Vector Machine (SVM). SVM has high accuracies with high-dimensional data. Still, linear separability is always an issue for that family of algorithms, and new dimensions need to be introduced to solve the problem. Hu 38 and Shi [8] created a time-series sequence of customer behaviors, fed this into an LSTM model, and then used the outcome as a new feature to be fed into a Random Forest model. Zhai et al. [9] used an ensemble model combining XGB and LightGBM algorithms to predict customer purchases on extensive e-commerce customer interaction data. Policarpo et al. [10] provided a comprehensive and up-to-date survey of machine learning techniques used in e-commerce platforms. Stubseid and Arandjelovic [11] represented the difference between the Naive Bayes approach and the RF approach using real-world data, which consists of a user to product relation. Finally, Sasi et al. [12] applied RFM and Recurrent Neural Network using customers' previous purchases to predict the next purchase by including the time factor.

It is clear from the literature that prediction of the next purchase and propensity of customers are becoming more critical in e-commerce to optimize customer-product relations and provide better options to customers. Differently from the rest of the studies in the literature, we investigate the effect of changing the target variable from order probability to click probability in brand propensity prediction. We find that click as a target variable is more beneficial in brand propensity prediction.

3. Proposed Brand Propensity Models and Methodology

In most of the propensity models, the main features are the aggregated actions of the users. In e-commerce environments, these actions are related to product: visit, favorite, basket, search, and order are the main interactions. The first four interactions constitute the signals of the customer for buying a product. They all show the customer's interest in a brand, category, and specifically in that product. Those signals which translate into an interest might turn into an order. Finally, the order itself is a strong signal as well. After a completed order based on the product category, the customer might continue ordering the same product or from the same brand/category.

An essential problem in brand propensity is related to the replenishment of the products. Every product has a different purchase frequency. So, in this model, a brand-based repurchase ratio is calculated for each product. And then, these constants are multiplied by the main features to scale the features by interaction ratios. The input and the target variables of the baseline model are shown in Table 1.

The idea is to sort those brands for each customer so that if they order a product the next day, that brand is in the top 5 brands listed for that customer by the model. The model is responsible for gathering those signals, giving different weights to those signals, and then calculating the order probability from that brand in the next 24 hours as the output. More specifically, the created dataset includes 2.153.360 rows and 40 columns. This data has been gathered from the users who visited the application. There are around 2 million users. Numerous attributes have been collected for each user transaction, such as the number of basket actions, likes, and orders a user made in the last one week, last one day, and last two weeks.

These features were built into an LR model [13] for predicting whether a customer has ordered based on his/her signals. So, an LR model is fit into the data using the Sklearn package in Python with the parameters listed in Table 2. LR has been preferred due to its performance on brand

Table 1. The input and output variables used by the baseline model

Type	Variable	Description	Time period
Input variable	Basket count (user-based)	Number of times a brand is added to basket	1d, 1w, 2w, 1m
	Favorite count (user-based)	Number of times a brand is favorited	1d, 1w, 2w, 1m
	Search count (user-based)	Number of times a brand is searched	1d, 1w, 2w, 1m
	Visit count (user-based)	Number of times a brand is visited	1d, 1w, 2w, 1m
	Order count (user-based)	Number of times a brand is ordered	1d, 1w, 2w, 1m
	Basket interaction with brand repurchase ratio	Basket count * brand repurchase ratio	1d, 1w, 2w, 1m
	Favorite interaction with brand repurchase ratio	Basket count * brand repurchase ratio	1d, 1w, 2w, 1m
	Search interaction with brand repurchase ratio	Basket count * brand repurchase ratio	1d, 1w, 2w, 1m
	Visit interaction with brand repurchase ratio	Basket count * brand repurchase ratio	1d, 1w, 2w, 1m
	Order interaction with brand repurchase ratio	Basket count * brand repurchase ratio	1d, 1w, 2w, 1m
Target variable	Brand ordered	Brand ordered the next one day.	1d

Table 2. Logistics Regression parameters for the sklearn function

Parameter	Value
Penalty	l2
Dual	False
Tol	0.0001
C	2.0
Fit intercept	True
Intercept scaling	1
Class weight	“balanced”
Random state	None
Max iteration	100
Multi class	‘ovr’
Verbose	1
Warm start	False

Table 3. Input and target variables of the CTR propensity model

Type	Variable	Description	Time period
Input variable	Click propensity score	Propensity probability from the 1st propensity model	1d
	CTR rates for each brand	CTR ratios for each brand based on widget metrics	1d
Target variable	Brand clicked	Brand clicked the next day	1d

propensity prediction and quick training times. For comparison purposes, models based on DT, RF, and XGB have also been developed. Next, we attempted to improve the performance of the baseline model by changing the target from order to click. The same features have been used to predict the click on the brand. Additionally, click-through rate (CTR) has been added to the model to increase the conversion rates further. And then, another model used the

outcome of the first baseline model and CTR to predict click again. So, this turned into an ensemble model called the CTR propensity model, as illustrated in Figure 1.

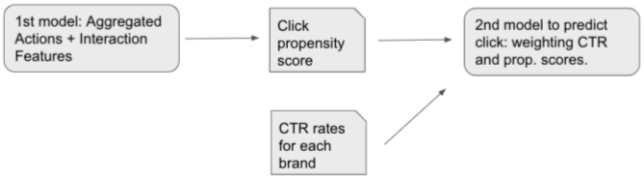

Figure 1. Improved ensemble CTR propensity model

In conclusion, the base model creates propensity scores for each user for the corresponding brands. But the ensemble model tunes the propensities using CTR data from the widget. This way, popular brand features are gathered and combined into the model. If some brands are more popular than the previous day, this overall aggregated feature is also integrated into the model. This feature is then used in the second model and thus tunes the propensity scores of the users.

CTR rates are calculated daily for the widget of the corresponding brand. Based on the signals obtained from the customers, raw propensity scores are weighted and rescored to produce the final output. Table 3 shows the input and target variables of the CTR propensity model.

The "Top N accuracy" metric [14] has been used to evaluate the performance of the models. The Trendyol application consists of different widgets. They correspond to a particular place in the application and have different functionalities. Figure 2 shows the brand slider widget in the Trendyol application. This widget is a slider in the application. It consists of brand logos that take the user to those brands if clicked. Brands in this slider are calculated and ordered by this algorithm in the paper. For each user, brand propensities are calculated and used to provide a personalized experience to the users. So, the brands and their order inside the widget are calculated by the corresponding user's interaction with the application. These interactions are used as features to predict the brand propensity of the user.

The "Top N" brands calculated are fed into this widget. Since the brand slider widget has limited slots for the brands, in both models, N was set to 5.

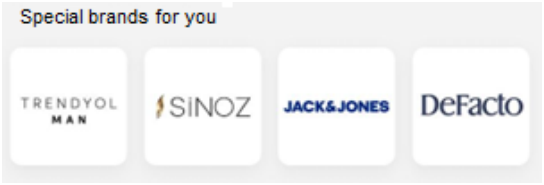

Figure 2. Brand slider widget in the Trendyol application

4. Results and Discussion

Table 4 shows the results achieved by evaluating the baseline and CTR propensity models. Since the order data is sparse, only customers with orders have been selected to assess the results of the models.

Table 4. Results achieved by evaluating the models using LR, DT, RF, and XGB (Top 3 and Top 5 product purchases - at least one transaction)

Model	Simulation Metric	Probability
LR-based Baseline model	Top 3 product purchase	57.36%
	Top 5 product purchase	65.05%
LR-based CTR propensity model	Top 3 product purchase	64.07%
	Top 5 product purchase	80.10%
DT-based CTR propensity model	Top 3 product purchase	61.09%
	Top 5 product purchase	69.33%
RF-based CTR propensity model	Top 3 product purchase	64.19%
	Top 5 product purchase	76.63%
XGB-based CTR propensity model	Top 3 product purchase	64.01%
	Top 5 product purchase	75.43%

According to the results obtained, when the "Top 3" product purchase metric is evaluated, the LR-based baseline and CTR propensity models yield an order probability of 57.36% and click probability of 64.07% for the next day, respectively. Similarly, when the "Top 5" product purchase metric is evaluated, the baseline and CTR propensity models produce an order probability of 65.05% and a click probability of 80.00% for the next one day, respectively.

In both "Top 3" and "Top 5" product purchase evaluations, it is observed that the CTR propensity model, where click is predicted as the target variable, clearly outperforms the baseline model predicting the order probability. The gain in probability obtained using the CTR propensity model instead of the baseline model is 11.69% and 22.98% for "Top 3" and "Top 5" product purchase metrics, respectively.

To compare and validate the accuracy of the LR-based CTR propensity prediction, models based on DT [15], RF [16], and XGB [17] have also been developed. When the "Top 3" product purchase metric is evaluated, the probabilities of DT-based, RF-based, and XGB-based models range from 61.09% to 64.19%. Similarly, when the "Top 5" product purchase metric is evaluated, the probabilities of DT-based, RF-based, and XGB-based models vary between 64.19% and 75.53%. Although LR shows comparable performances to other alternative methods in terms of "Top 3" product purchase metric, it clearly outperforms other methods in terms of the "Top 5" product purchase metric.

We can conclude that click as a target variable, an indirect way to increase the order rates, came out as more beneficial. The results have shown that the CTR propensity model can sort brands in such a way that the calculated "Top 5" brands for users with at least one order have an acceptable high probability (i.e., 80.00%) of being that ordered brand.

5. Conclusion and Future Work

This study investigated the effect of the target variable on brand propensity prediction using LR. For comparison purposes, models based on DT, RF, and XGB have also been developed. The target variable to be evaluated has been set to both order and click probabilities. The users' interactions (i.e., product visit, favorite, basket, search, and order) constitute the signals/features for the models to interpret. They are aggregated by brand and used to predict the brand's order and click probabilities. The results show that click as a target variable, an indirect way to increase the order rates, has been revealed to be more beneficial in predicting brand propensity. In addition, the LR-based CTR propensity model exhibits the best average performance among the machine learning methods for both Top 3 and Top 5 product purchases.

In the future, we plan to evaluate other promising methods, such as general regression neural networks and multilayer perceptron, which can be leveraged to improve the prediction accuracy of brand propensity. Also, other candidate potential features, such as customers' past purchase history and location, can be integrated into our prediction models to investigate the correlation of these variables with brand propensity.

Declaration of Ethical Standards

The author(s) of this article declare that the materials and methods used in this study do not require ethical committee permission and/or legal-special permission.

Conflict of Interest

The authors declare that they have no known competing financial interests or personal relationships that could have appeared to influence the work reported in this paper.

References

[1] Hussien F. T. A., Rahma A. M. S., Abdulwahab H. B., 2021. An e-commerce recommendation system based on dynamic analysis of customer behavior, Sustainability, **13**(19), 10786.

[2] Abdul Hussien F. T., Rahma A. M. S., Abdul Wahab H. B., 2021. Recommendation Systems for E-commerce Systems An Overview. Journal of Physics: Conference Series, **1897**(1), 012024.

[3] Daoud M., Naqvi S. K., Ahmad A., 2014. Opinion Observer: Recommendation System on E-Commerce Website. International Journal of Computer Applications, **105**(14), pp. 975–8887.

[4] Zhang Y., 2021. Prediction of Customer Propensity Based on Machine Learning. In: Proceedings of Asia-Pacific Conference on Communications Technology and Computer Science, pp. 5–9.

[5] Valecha H., Varma A., Khare I., Sachdeva A., Goyal M., 2018. Prediction of Consumer Behaviour using Random Forest Algorithm. In: Proceedings of 5th IEEE Uttar Pradesh Section International Conference on Electrical, Electronics and Computer Engineering, pp. 1-6.

[6] Szabó P., Genge B., 2020. Efficient Conversion Prediction in E-Commerce Applications with Unsupervised Learning. In: Proceedings of 28th International Conference on Software, Tele-communications and Computer Networks.

[7] Liu X., Li J., 2016. Using support vector machine for online purchase predication. In: Proceedings of International Conference on Logistics, Informatics and Service Sciences.

[8] Hu W., Shi Y., 2020. Prediction of online consumers' buying behavior based on LSTM-RF model. In: Proceedings of 5th International Conference on Communication, Image and Signal Processing, pp. 224–228.

[9] Zhai X., Shi P., Xu L., Wang Y., Chen X., 2020. Prediction Model of User Purchase Behavior Based on Machine Learning. In: Proceedings of IEEE International Conference on Mechatronics and Automation, pp. 1483–1487.

[10] Micol P. L. et al., 2021. Machine learning through the lens of e-commerce initiatives: An up-to-date systematic literature review, Computer Science Review, **41**, 100414.

[11] Stubseid S., Arandjelovic O., 2018. Machine Learning Based Prediction of Consumer Purchasing Decisions: The Evidence and its Significance. In: Workshops of the Thirty-Second AAAI Conference on Artificial Intelligence, pp. 100–106.

[12] Sasi R. K., John H., Jerard B., Sudheer S., A. Shaju, 2020. Customer Behaviour Prediction using Propensity Model. IPEM Journal of Computer Application & Research, **5**, pp. 38–43.

[13] Peng C. Y. J., Lee K. L., Ingersoll G. M., 2010. An Introduction to Logistic Regression Analysis and Reporting. The Journal of Educational Research, **96**(1), pp. 3–14.

[14] Cremonesi P., Koren Y., Turrin R., 2010. Performance of recommender algorithms on top-N recommendation tasks. In: Proceedings of the 4th ACM Conference on Recommender Systems, pp. 39–46.

[15] Lakshminarayanan B., Decision Trees and Forests: A Probabilistic Perspective, Ph.D. Thesis, 2016.

[16] Ali J., Khan R., Ahmad N., Maqsood I., 2012. Random Forests and Decision Trees. International Journal of Computer Science Issues, **9**(5), pp. 272–278.

[17] Chen T., Guestrin C., 2016. XGBoost: A scalable tree boosting system. In: Proceedings of the ACM SIGKDD International Conference on Knowledge Discovery and Data Mining, pp. 785–794.

Koc. J. Sci. Eng., 5(ICOLES2021): (2022) 38-47 https://doi.org/10.34088/kojose.1015129

Kocaeli University

Kocaeli Journal of Science and Engineering

http://dergipark.org.tr/kojose

Integrated Entropy-EDAS Methods for the Electrified Car Selection Problem

Elif ÇALOĞLU BÜYÜKSELÇUK [1,*], Hakan TOZAN [2]

[1] *Department of Industrial Engineering, Fenerbahçe University, İstanbul, 34758, Turkey,* ***ORCID:*** *0000-0002-5976-6727*
[2] *Department of Industrial Engineering, İstanbul Medipol University, İstanbul, 34810, Turkey,* ***ORCID:*** *0000-0002-0479-6937*

Article Info

Research paper

Received : *October 26, 2021*
Accepted : *June 06, 2022*

Keywords

Air Pollution
Decision Making
EDAS
Electrified Car
Entropy

Abstract

Increasing air pollution affects the environment and life negatively. For a sustainable environment and life, people, voluntary organizations, and governments need to work on the solution of this problem. The biggest sources of air pollution are transportation vehicles. For this reason, many countries in Europe have stated that they will use solely electrified cars to reduce air pollution in the future. Therefore, in this study, it is aimed to determine the best electrified car. The result obtained can support consumers that to intend to buy an electrified vehicle in the decision-making process. This problem is a typical multi-criteria decision making (MCDM) problem and some MCDM techniques are used to solve these problems. Here, the Entropy method was used to determine the weights of the selection criteria. Selection criteria was determined according to comprehensive literature survey and interviews with sales representatives. The EDAS (Evaluation based on Distance from Average Solution) method was used to rank the electrified car alternatives that sold in Turkey. As a result of the evaluation, the most important criteria was determined by the price of the vehicle, the net battery capacity, and the electric motor power. According to these criteria, the electrified car manufactured in China was chosen as the best.

1. Introduction

According to the statement made by the World Health Organization, air pollution seriously threatens human life and causes the death of approximately two million people worldwide every year. Our world is becoming uninhabitable due to rapidly increasing population growth, unplanned urbanization, industrialization, and many reasons [1]. If cautions are not taken to solve this problem, there will be no world in which we can live in the future.

As a result of increasing greenhouse gases, climate change threatens the whole world. The biggest factor in the increase of greenhouse gases is due to the exhaust gases thrown into the air from transportation vehicles especially in big cities [2]. For this reason, automobile manufacturers have started to use electric motors instead of internal combustion engines in their cars for a cleaner environment. The world will become more livable due to the usage of electric vehicles with zero CO_2 emissions [3]. Not only manufacturers, but also governments have started to act. For this reason, many countries have announced that they will ban the sale of cars using gasoline and diesel fuel. In 2016, Norway announced that the sale of these cars would be banned as of 2025, while on the same dates it announced that it would implement a similar application in Germany from 2030. With this decision, the country aims to reduce its CO_2 emissions by 95% by 2050. Following these countries, France, England, Scotland, the Netherlands, and many European countries have announced that they will follow the same policy [4]. Such policies have brought the production, sale, and use of electric vehicles all over the world, especially in Europe, to the agenda. As a result of these sanctions, the determination of the most efficient electrified car is also an important issue.

In this study, it is aimed to determine the best electric cars among alternatives sold in Turkey. This is a typical multi-criteria decision making problem and integrated Entropy and EDAS methods are used to solve the problem.

* Corresponding Author: elif.buyukselcuk@fbu.edu.tr

A limited number of studies have been reached in the literature on electric vehicles evaluation and selection process. Xue et al., in their study in 2008, tested six different types of drivetrain systems used in the engines of electric vehicles [5]. On the other hand, Baghdadi et al. examined the electric vehicles of two different brands such as Peugeot iOn and Ford Transit Connect in 2013 and tested their current battery capacities, ranges and battery charging times under real road and laboratory conditions [6]. In Scandinavia, an electrical car model was evaluated according to its range in the different weather conditions [7].

In this study, the selection problem was handled by using different MCDM techniques. In the literature, there are many studies that used these techniques for various sector. Zou and his colleagues used the Entropy method to determine the weights of the criteria in the water quality assessment in 2006 [8]. In 2017, the machines were evaluated according to twelve criteria to determine the best one among the three different machines. While the Entropy method was used to calculate the criteria weights, the best machine was determined by the SAW method [9]. To determine the appropriate supplier, it was aimed to weight the criteria objectively in the study using the Entropy and AHP-based TOPSIS method [10]. Lahsini evaluated smartphones in terms of seven qualitative features in his study in 2017. He solved the problem by using the Entropy and MAUT (Multi-Attribute Utility Theory) methods together [11]. In another study, performance criteria were determined as the first step in measuring the performance of companies operating in the automotive sector and traded on the Istanbul stock exchange. Entropy method was used to weight the performance criteria. The weights obtained were first used in MAUT and then in SAW methods, and the performances of the companies were evaluated and ranked [12]. Nyimbili and Erden developed a hybrid model to evaluate emergency facility planning in Istanbul in their study in 2020. AHP and Entropy methods were used to determine the weights of the criteria objectively and subjectively [13]. Kenger (2017) dealt with the bank personnel selection problem in his thesis. In the solution of the problem, he made evaluations by using different MCDM techniques together [14]. Özbek and Engür (2018) used the EDAS method to evaluate the websites of companies operating in the logistics sector. They determined criteria like web site language, customer relations, online ordering, visual content etc. and they assumed that all criteria have the same weight [15]. In energy sector, for high efficiency a MCDM model was developed to evaluate five renewable resources. The criteria weights were calculated by using Shannon Entropy method and EDAS method was applied for selection of energy resources [16]. Yalçın and Uncu (2019) applied EDAS method to validate industrial robot selection process. They examined four different examples in their study. They found that EDAS is suitable method for right industrial robot selection [17]. Mitra used EDAS method for cotton fabric selection process in 2020. 13 different alternatives were evaluated according to four different criteria (cover, thickness, areal density, porosity) [18]. He and his colleagues studied to determine and evaluate green supplier by using information entropy and EDAS under uncertainty. The novel model developed by them was very easy to understand and compute [19]. For a construction project, fuzzy EDAS was used to determine the best company among five according to four different criteria. Technical, management, financial and time are the main factors [20]. Mathew and Sahu (2018) compared four alternatives to determine the most suitable conveyor according to six different criteria. In the selection process, fixed cost, variable cost, conveyor speed, product width, product weight and flexibility criteria were used. They used to EDAS method for the selection process [21]. The EDAS method was also used in material selection in the automotive industry. Different alternatives were evaluated according to different criteria and the result was reached [22]. Different multi-criteria decision-making techniques and their application areas are summarized in Table 1.

Finally, it has been observed that multi-criteria decision-making methods are used in many different areas and in solving many different problems. During the solution process, it has been witnessed those different methods work together. However, no study has been found in the literature on which criteria are important in the selection of electric vehicles and in the measurement of their performance, and which of the existing vehicles is the best. This study was designed to fill this gap. In order to fill this gap, it is aimed to select the best electrified vehicles available in the market by using Entropy-based EDAS methods in the selection process. After the criteria were determined, the Entropy method was used to determine their weights. The Entropy method is one of the most frequently used and easy method for implementation. The higher difference in value between alternatives while evaluating on the same criterion, the more important that criterion is. The more useful a criterion is, it plays the greater role in decision making. If a criterion has equal value among the alternatives, that criterion is disabled during the evaluation process, indicating that the weight of that criterion will be zero. EDAS method, which is used to determine the best alternative by finding the distance from the average solution, is different from other MCDM methods based on the logic of the compromise approach.

Table 1. Different MCDM methods and application areas.

Author(s)	Methods	Application area
Caloglu Buyukselcuk [23]	AHP-VIKOR integrated method	Food industry
Hussain and Mandal [24]	Entropy based COPRAS and MOORA	Material selection
Ersoy [25]	Entrophy-TOPSIS and GRA integrated methods	White goods industry
Ocampo et. al. [26]	Fuzzy DEMATEL-ANP-TOPSIS	Food Manufacturing
Kaviani et. al. [27]	Grey-Shannon entropy, grey EDAS	Oil and gas industry
Yazdani et. al. [28]	FMEA, EDAS	Construction industry
Galankashi et. al. [29]	Mixed Balanced Scorecard and fuzzy AHP	Automobile industry
Liu et. al. [30]	DEMATEL based ANP with VIKOR	Evaluating employee care strategies
Prakash and Barua [31]	Fuzzy AHP and VIKOR	Indian electronics industry
Mohammed et. al. [32]	ELECTRE and TOPSIS	Vendor selection
Dweiri et. al. [33]	Integrated AHP based decision support system	Automobile industry in Pakistan
Merdivenci and Oğuz [34]	Entropy based EDAS method	Personnel selection in logistics sector
Özaydın and Karakul [35]	Entropy with MAUT, SAW and EDAS	Financal analysis in food and beverages sector
Ali et. al. [36]	Integrated Entropy and EDAS methods	Renewable energy technology selection in energy sector

2. Materials and Methods

In this study, it is aimed to measure the performance of electric cars offered for sale in Turkey by using integrated Entropy and EDAS methods. In the first step, because of literature review and research, the criteria to be considered when buying an electric car were determined and these criteria were grouped according to beneficial and non-beneficial. Then, electrified car of different brands and models sold in Turkey were determined. For the criteria of these cars determined in the second step, a decision matrix was created by obtaining data from the official web sites and catalagoues of the vehicles. The weights of all variables were determined using the Entropy method. In the third step, the performances of existing electrified cars were evaluated using the EDAS method and these vehicles were ranked. As a result of this ranking, the best electrical cars sold in the market were determined. In this section, the beneficial and non-beneficial variables considered in the study and the techniques used in problem solving will be discussed. The flow chart for this problem was represented (Figure 1).

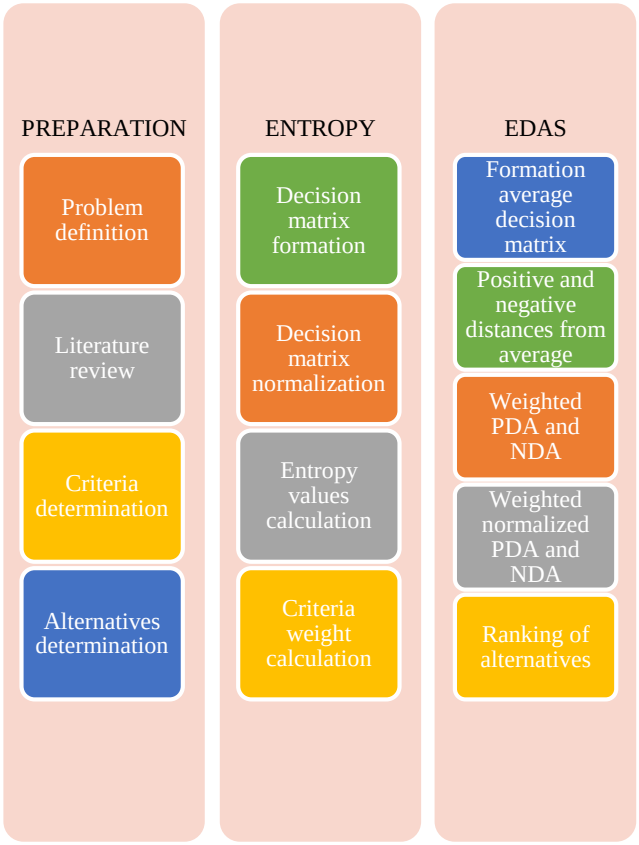

Figure 1. Flow chart of the problem

2.1. Determination of Criteria

By reviewing the literature on the subject and examining the forum pages of electric vehicles, the official websites and technical catalogs of brands that sell electrified cars, and by interviewing car sales representatives, it has been determined which criteria should be considered when buying electric vehicles.

The guarantee of the battery used in the vehicles, the net battery capacity, the charging time of the battery, the power of the electric motor, the maximum torque of the electric motor, the unloaded weight of the vehicle, the price of the vehicle, the vehicle's range, maximum speed, acceleration performance and energy consumption are considered as selection criteria. Since the CO_2 emission value of the vehicles is zero in all electric vehicles, this parameter is not considered as a criterion.

Criteria are summarized and categorized due to beneficial or non-beneficial (Table 2).

Table 2. Criteria definitions, codes, and types.

Criteria Name and Code	Type
Battery warranty (km)-C1	Beneficial
Net battery capacity (kW-h)-C2	Beneficial
Charging time (minute)-C3	Non-beneficial
Electric motor power (BG)-C4	Beneficial
Maximum torque (Nm)-C5	Beneficial
Unloaded weight (kg)-C6	Non-beneficial
Price (TL)-C7	Non-beneficial
Range (km)-C8	Beneficial
Maximum speed (km/h)-C9	Beneficial
Acceleration time (second)-C10	Non-beneficial
Consumption (kW-h/100 km)-C11	Non-beneficial

Electric car manufacturers guarantee their batteries for a certain year or a certain range of use. In general terms, battery capacity is the energy contained in the battery in the electric vehicle. This value is as important as the torque and engine power of the vehicle because the size of the battery used, its capacity and how efficiently it is used affect the range of the vehicle [37]. There are different types and levels of charging for the battery to charge. In this study, the type of long-term charging is considered [38]. The task of the electric motor in electric vehicles is to give traction to the wheels by converting the energy provided by the battery into mechanical energy. The driving force for an electric motor is torque. The unit of torque is expressed in Newton-meters. Torque is the parameter that enables vehicles to reach higher speeds in a short time during acceleration and ensures that the traction of the vehicle is strong [39]. Weight is also an important criterion in electric vehicles. Higher efficiency is achieved by producing vehicles with less weight by using lighter materials with the same battery capacity. In addition to all performance-related criteria, the price of the vehicle is one of the criteria considered by the end users. Continuous improvement efforts are being made to increase range in electric vehicles [40]. The maximum distance that the vehicle can travel with a fully charged battery is another criterion considered by users. One of the questions frequently asked by users during vehicle purchase is the maximum speed of the vehicle. The acceleration value of the vehicle is determined by expressing the time in seconds for the vehicle to reach 100 km speed from the moment of stopping [41]. Another critical point that users pay attention to when purchasing a vehicle is how much energy the vehicle will consume for a range of 100 km.

2.2. Entropy Method

In this part, the steps of the Entropy method used to determine the weights of the criteria will be explained. The entropy method is one of the objective weight methods and is frequently used in the literature. One of the most important advantages of the entropy method is that it eliminates the necessity of using the intuitive approach and verbal judgments of decision makers [42]. The steps of the method are as given below [43, 44]:

Step 1. The decision matrix is created by determining the performance values of each of the alternatives for different criteria.

$$X = [x_{ij}] = \begin{bmatrix} x_{11} & x_{12} & \dots & x_{1n} \\ x_{21} & x_{22} & \dots & x_{2n} \\ \vdots & \vdots & \ddots & \vdots \\ x_{m1} & x_{m2} & \dots & x_{mn} \end{bmatrix} \quad (1)$$

where x_{ij} is the performance value of i_{th} alternative according to j_{th} criterion ($i = 1,2,\dots,m$ and $j = 1,2,\dots,n$).

Step 2. The decision matrix is normalized using the following equation so that all variables that make up the decision matrix are comparable and dimensionless. Eq. (2) is used for this purpose.

$$r_{ij} = \frac{x_{ij}}{\sum_{i=1}^{m} x_{ij}} \quad (2)$$

Step 3. Entropy values are calculated for each criterion by using Eq. (3). e_j is the entropy value of j_{th} criterion. e_j values must satisfy the condition of $0 \leq ej \leq 1$.

$$e_j = -k \cdot \sum_{i=1}^{m} r_{ij} \cdot ln\,(r_{ij}) \quad (3)$$

where k is the entropy coefficient and is calculated by using Eq. (4).

$$k = (ln\,(n))^{-1} \quad (4)$$

Step 4. By using Eq. (6), entropy weights are determined.

$$w_j = \frac{1 - e_j}{\sum_{j=1}^{n}(1 - e_j)} \quad (5)$$

$$\sum_{j=1}^{n} w_j = 1 \quad (6)$$

$1 - e_j$ represents the degree of difference of each criterion's intrinsic information. The normalization of $1 - e_j$ values, the final entropy weights of criteria are determined. If a criterion has the smallest entropy value, it will have the greatest entropy weight.

2.3. EDAS Method

EDAS was developed by Keshavarz Ghorabaee and his colleagues in 2015 [45]. They tested the validity of the method by comparing it with other MCDM techniques such as VIKOR, TOPSIS, SAW and COPRAS. The steps of EDAS are given below [15, 46]:

Step 1. After the decision matrix containing the values of the alternatives according to the criteria is created, the average value due to all the criteria is determined using Eq. (7).

$$AV_j = \frac{\sum_{i=1}^{m} x_{ij}}{m} \quad (7)$$

$$AV = [AV_j]_{1xn} \quad (8)$$

Step 2. The positive distance and negative distance matrices from the average for each criterion are shown as expressed in the Eq. (9) and Eq. (10). Positive and negative distances from the average are calculated using Eq. (11), Eq. (12), Eq. (13) and Eq. (14) according to the types of criteria.

$$PDA = [PDA_{ij}]_{mxn} \quad (9)$$

$$NDA = [NDA_{ij}]_{mxn} \quad (10)$$

For beneficial criteria:

$$PDA_{ij} = \frac{max\,(0,(x_{ij} - AV_j))}{AV_j} \quad (11)$$

$$NDA_{ij} = \frac{max\,(0,\ (AV_j - x_{ij}))}{AV_j} \quad (12)$$

For non-beneficial criteria:

$$PDA_{ij} = \frac{max\,(0,(AV_j - x_{ij}))}{AV_j} \quad (13)$$

$$NDA_{ij} = \frac{max\,(0,\ (x_{ij} - AV_j))}{AV_j} \quad (14)$$

Step 3. The weighted total PDA and NDA are calculated for each alternative. v_j is the weight of j_{th} criterion.

$$SP_i = \sum_{j=1}^{n} v_j \,.\, PDA_{ij} \quad (15)$$

$$SN_i = \sum_{j=1}^{n} v_j \,.\, NDA_{ij} \quad (16)$$

Step 4. SP ve SN values are normalized for each alternative by using Eq. (17) and Eq. (18).

$$NSP_i = \frac{SP_i}{max_i\,(SP_i)} \quad (17)$$

$$NSN_i = 1 - \frac{SN_i}{max_i\,(SN_i)} \quad (18)$$

Step 5. Assessment score (AS_i) is calculated for all alternatives by using Eq. (19). AS_i values must satisfy the condition of $0 \leq AS_i \leq 1$.

$$AS_i = \frac{1}{2}\,(NSP_i + NSN_i) \quad (19)$$

Step 6. Alternatives are ranked by AS_i value from largest to smallest. The alternative in the first place is determined as the best one.

3. Results and Discussion

In this study, integrated entropy and EDAS methods were used to determine the best electric vehicles sold in Turkey. Electric SUVs available in the market were not among the alternatives in the study. Only electrified cars have been identified as alternatives. Three of these are vehicles from German, one from Chinese and the other from French automakers. As a result of the literature review, the criteria to be considered when buying an electric car were determined, and the Entropy method, which is one of the objective methods, was used to determine the weights of these criteria. Using the EDAS method, the best electrified car was determined.

3.1. Determination of the Criteria Weight via Entropy Method

After determining the initial decision matrix of the criteria and alternatives obtained from their technical catalogues and official web sites (Table 3), a normalized decision matrix was created by using Eq. (2) and Eq. (3). Normalized matrix results have been represented in Table 4. The entropy values and entropy weights for each criterion were calculated using Eq. (4) and Eq. (6) and have been shown in Table 5.

When Table 5 is examined, it is seen that the criterion with the largest entropy value has the least entropy weight value. According to these results, it is seen that the most important evaluation criterion is the price of the car ($w_j = 0.126$). It is followed by electric motor power, net battery capacity and battery charging time, respectively. Maximum speed, unloaded weight and battery warranty are the criteria with the lowest weight.

Table 3. Initial decision matrix.

	C1	C2	C3	C4	C5	C6	C7	C8	C9	C10	C11
A1	100,000	37.9	490	170	250	1345	704,000	310	150	7.3	14.2
A2	100,000	17.6	193	82	160	1085	156,000	160	130	12.7	16
A3	100,000	52	565	108	225	1577	368,900	395	135	11.4	17.2
A4	150,000	40	500	114	270	1460	283,000	320	130	9.5	15
A5	160,000	71	570	408	357	2130	2,200,000	390	230	5.4	28.7

Table 4. Normalized matrix.

	C1	C2	C3	C4	C5	C6	C7	C8	C9	C10	C11
A1	0.164	0.173	0.208	0.193	0.198	0.177	0.190	0.197	0.194	0.158	0.156
A2	0.164	0.081	0.084	0.093	0.127	0.143	0.042	0.102	0.168	0.274	0.176
A3	0.164	0.238	0.245	0.122	0.178	0.208	0.099	0.251	0.174	0.246	0.189
A4	0.246	0.183	0.217	0.129	0.214	0.192	0.076	0.203	0.168	0.205	0.165
A5	0.262	0.325	0.247	0.463	0.283	0.280	0.593	0.248	0.297	0.117	0.315

Table 5. Entropy values and entropy weights.

	C1	C2	C3	C4	C5	C6	C7	C8	C9	C10	C11
Entropy values (e_j)	0.661	0.636	0.649	0.591	0.658	0.661	0.494	0.654	0.660	0.653	0.655
Entropy weights (w_j)	0.0841	0.0904	0.0872	0.1016	0.085	0.0842	0.1256	0.0858	0.0845	0.086	0.0856

3.2. Determination of the Best Electrified Car via EDAS

The performances of these cars according to the evaluation criteria have been obtained from the official websites. The data set and the average value of the decision problem (by using Eq. (7)) have been given in Table 6. Positive and negative distance values from the average (PDA and NDA) were calculated using Eq. (11)-Eq. (12) and have been shown in Table 7 and Table 8. Weighted total PDA and NDA values for each alternative were calculated using Eqs. 15 and 16. The criteria weights used here were predetermined by the Entropy method. The obtained SP_i and SN_i values were normalized using Eq. (17)-Eq. (18) and the results are summarized in the Table 9.

Table 6. Data set of the problem and average values.

	C1	C2	C3	C4	C5	C6	C7	C8	C9	C10	C11
A1	100,000	37.9	490	170	250	1345	704,000	310	150	7.3	14.2
A2	100,000	17.6	193	82	160	1085	156,000	160	130	12.7	16
A3	100,000	52	565	108	225	1577	368,900	395	135	11.4	17.2
A4	150,000	40	500	114	270	1460	283,000	320	130	9.5	15
A5	160,000	71	570	408	357	2130	2,200,000	390	230	5.4	28.7
Average	122,000	43.7	461.6	176.4	252.4	1519.4	742,380	315	155	9.26	18.22

Table 7. Positive distance values from average (PDA_{ij}).

PDA_{ij}	C1	C2	C3	C4	C5	C6	C7	C8	C9	C10	C11
A1	0	0	0	0	0	0.115	0.052	0	0	0.212	0.221
A2	0	0	0.582	0	0	0.286	0.790	0	0	0	0.122
A3	0	0.190	0	0	0	0	0.503	0.254	0	0	0.056
A4	0.230	0	0	0	0.070	0.039	0.619	0.016	0	0	0.177
A5	0.311	0.625	0	1.313	0.414	0	0	0.238	0.484	0.417	0

Table 8. Negative distance values from average (NDA_{ij}).

NDA_{ij}	C1	C2	C3	C4	C5	C6	C7	C8	C9	C10	C11
A1	0.180	0.133	0.040	0.036	0.010	0	0	0.016	0.032	0	0
A2	0.180	0.597	0	0.535	0.366	0	0	0.492	0.161	0.371	0
A3	0.180	0	0.224	0.388	0.109	0.038	0	0	0.129	0.231	0
A4	0	0.085	0.083	0.354	0	0	0	0	0.161	0.026	0
A5	0	0	0.235	0	0	0.402	1.963	0	0	0	0.575

Table 9. SP_i, SN_i and normalized NSP_i, NSN_i values.

	SP_i	NSP_i	SN_i	NSN_i
A1	0.053	0.153	0.039	0.888
A2	0.184	0.529	0.242	0.308
A3	0.107	0.307	0.117	0.665
A4	0.123	0.352	0.067	0.810
A5	0.348	1	0.350	0

After the normalized SP and SN values were determined, the assessment score was calculated for each alternative using Eq. (19).

Considering all criteria, it has been determined that the electric car produced in China is the best. In the second and third place, it was determined that the electrified cars produced in Germany were the best (Figure 2). While some researchers discuss that the use of electric vehicles will prevent air pollution, some researchers argue the opposite. However, it is clear that the use of electric vehicles in the long term is one of the important steps to be taken in preventing air pollution [47, 48, 49].

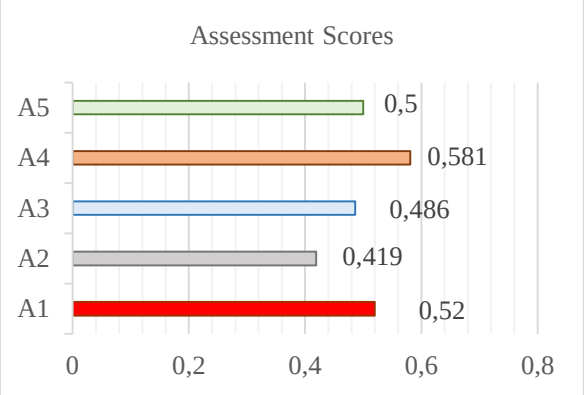

Figure 2. Assessment scores of alternatives.

4. Conclusions

With this study, it has been underlined once again that some necessary precautions for a sustainable life should be taken. To put a stop to air and environmental pollution that threatens the whole world, governments need to take urgent measures and impose sanctions on a local and global scale. In recent years, some measures should be taken urgently to prevent air pollution, which adversely affects the health of the whole world. While the rapidly increasing population, wrong urbanization, a noticeable increase in the use of pesticides and chemicals cause air pollution, another factor is the exhaust gases from the vehicles. Especially in the last eighteen months, there have been serious decreases in human activities due to the COVID-19 pandemic all over the world. This gave nature the opportunity to renew itself. One of the biggest factors in air pollution is undoubtedly vehicle traffic, and as it can be seen, the decrease in vehicle use plays an important role in air pollution control. Alternative ways to reduce emissions need to be found not only in automobiles, but also in factories, vehicles such as aircraft and ships. At this point, experts argue that with the increase in the use of electric cars, air pollution will decrease significantly. For this reason, many countries, especially Europe, have declared that they will ban the use of electric cars in the future and encourage their citizens to use these cars.

For this reason, most of the automobile manufacturers have produced and sold vehicles such as cars and SUVs that work with 100% electricity. For consumers, the critical question here is which vehicle will they buy? This problem is a multi-criteria decision-making problem and can be solved using MCDM techniques. In this study, the problem of choosing the best one among only electric cars sold in Turkey is discussed. First, it was determined which criteria would be considered while making the selection. The weights of these criteria were calculated using the Entropy method. As a result of the calculation, it has been determined that the first criterion to be considered in the process of purchasing and choosing an electrified car is the price. Other important criteria are electric motor power, net battery capacity and battery charging time, respectively.

Five electric cars of different brands sold in Turkey have been identified. After determining the data of these cars for the determined criteria, it was aimed to select the best one using the EDAS method. As a result of the evaluation, it has been determined that the vehicle produced in China is the best. In fact, this selected car is the second-cheapest car among all other models. The fact that price is the most important criterion is also a factor of this result. Although the second alternative is the cheapest vehicle in terms of price, however it is the weakest among the other models in terms of net battery capacity and electric motor power.

Since the price is such an important factor, the reorganization of taxes in terms of incentives for the sale

of electric vehicles will ensure that these vehicles are sold and used more. Another important criterion is the charging time of the battery. At this point, it is important to increase and expand the number of charging stations. There are still deficiencies in the number of charging stations in our country, especially in the Central Anatolia and Eastern Anatolia Regions on highways. It is inevitable to take measures for a sustainable life in Turkey. The use of electric vehicles should be encouraged, and the necessary infrastructure opportunities should be expanded, and new regulations should be made on taxes. Thus, activities aimed at reducing air pollution will be supported.

The lower performance of electric cars compared to internal combustion engine vehicles is a limiting factor. For this reason, research and development activities regarding electric vehicles continue intensively. When the performance of vehicles is increased with technological developments, the use of these vehicles may become more common. In the future, this problem can be solved under different evaluation criteria. In addition, comparisons can be made by evaluating with different MCDM techniques. The sale of electrified vehicles in Turkey is still very new and not very common. For this reason, the experiences and feedbacks of the users were not included in the evaluation and determination of the criteria. In the next study, it is planned to expand the evaluation criteria pool by taking into account the user feedback and the advantages and disadvantages of the use of electrified vehicles. In addition, there are currently a limited number of electric vehicles from a limited number of automakers. In the future, it will be possible to work with a wider alternative pool of electric vehicles of different brands and models.

Declaration of Ethical Standards

The author of this article declare that the materials and methods used in this study do not require ethical committee permission and/or legal-special permission.

Conflict of Interest

The authors declare that they have no known competing financial interests or personal relationships that could have appeared to influence the work reported in this paper.

References

[1] Choudhary, M. P., Garg, V., 2013. Causes, Consequences and Control of Air Pollution, Conference: All India Seminar on Methodologies for Air Pollution Control, India.

[2] Lozhkin, V., Lozhkina, O., Dobromirov, V., 2018. A Study of Air Pollution by Exhaust Gases from Cars in Well Courtyards of Saint Petersburg. Transportation Research Procedia, **36**, pp. 453 – 458.

[3] Efendi, A., Fahmi, A. R., 2021. Design and Build of Electric Car Frame SULA Evolution. Journal of Mechanical Engineering Education, **6**(1), pp. 11 – 21.

[4] Shammut, M., Cao, M., Zhang, Y., Papaix, C., Liu, Y., Gao, X., 2019. Banning Diesel Vehicles in London: Is 2040 Too Late?. Energies, **12**(3495), pp. 1 – 17.

[5] Xue, X. D., Cheng, K. W. E., Cheng, N. C., 2008. Selection of Electric Motor Drives for Electric Vehicles, Australasian Universities Power Engineering Conference, Australia, pp. 1 – 6.

[6] Baghdadi, M. E., Vroey, L. D., Coosemans, T., Mierlo, J. V., Foubert, W., Jahn, R., 2013. Electric Vehicle Performance and Consumption Evaluation. World Electric Vehicle Journal, **6**, pp. 30 – 37.

[7] Laurikko, J., Granström, R., Haakana, A., 2012. Assessing Range and Performance of Electric Vehicles in Nordic Driving Conditions. World Electric Vehicle Journal, **5**, 45 – 50.

[8] Zou, Z., Yun, Y., Sun, J., 2006. Entropy Method for Determination of Weight of Evaluating Indicators in Fuzzy Synthetic Evaluation for Water Quality Assessment. Journal of Environmental Sciences, **18**(5), pp. 1020 – 1023.

[9] Özdağoğlu, A., Yakut, E., Bahar, S., 2017. Machine Selection in a Diary Product Company with Entropy and SAW Methods Integration. Dokuz Eylül Üniversitesi İktisadi ve İdari Bilimler Fakültesi Dergisi, **32**(1), pp. 341 – 359.

[10] Chen, C. H., 2020. A Novel Multi-Criteria Decision-Making Model for Building Material Supplier Selection Based on Entropy-AHP Weighted TOPSIS. Entropy, **22**(2), pp. 1 – 23.

[11] Lahsini, L., 2017. Maut Yöntemi Kombinasyonunda Entropi Yöntemine Göre Ağırlıklandırma. Akademik Sosyal Araştırmalar Dergisi, **5**(41), pp. 501 – 512.

[12] Ömürbek, N., Karaatlı, M., Balcı, H. F., 2016. Entropi Temelli MAUT ve SAW Yöntemleri ile Otomotiv Firmalarının Performans Değerlemesi. Dokuz Eylül Üniversitesi İktisadi ve İdari Bilimler Fakültesi Dergisi, **31**(1), pp. 227 – 255.

[13] Nyimbili, P. H., Erden, T., 2020. A Hybrid Approach Integrating Entropy-AHP and GIS for Suitability Assessment of Urban Emergency Facilities.

International Journal of Geo-Information, **9**(419), pp. 1 – 29.

[14] Kenger, M. D., 2017. Banka Personel Seçimin Çok Kriterli Karar Verme Yöntemlerinden Entropi Temelli MAUT, ARAS ve Gri İlişkisel Analiz Yöntemleri ile Değerlendirilmesi. Yüksek Lisans Tezi, Pamukkale Üniversitesi, İşletme Anabilim Dalı, Denizli.

[15] Özbek, A., Engür, M., 2018. EDAS Yöntemi ile Lojistik Firma Web Sitelerinin Değerlendirilmesi. Selçuk Üniversitesi Sosyal Bilimler Meslek Yüksekokulu Dergisi, **21**(2), pp. 417 – 429.

[16] Yazdani, M., Torkayesh, A. E., Santibanez-Gonzalez, E. Dr., Otaghsara, S. K., 2020. Evaluation of Renewable Energy Resources Using Integrated Shannon Entropy-EDAS Model. Sustainable Operations and Computers, **1**, pp. 35 – 42.

[17] Yalçın, N., Uncu, N., 2019. Applying EDAS as an Applicable MCDM Method for Industrial Robot Selection. Sigma Journal of Engineering and Natural Sciences, **37**(3), pp. 779 – 796.

[18] Mitra, A., 2020. Selection of Cotton Fabrics Using EDAS Method. Journal of Natural Fibers, pp. 1-13.

[19] He, Y., Lei, F., Wei, G., Wang, R., Wu, J., Wei, C., 2019. EDAS Method for Multiple Attribute Group Decision Making with Probabilistic Uncertain Linguistic Information and Its Application to Green Supplier Selection. International Journal of Computational Intelligence Systems, **12**(2), pp. 1361 – 1370.

[20] Stanujkic, D., Zavadskas, E. K., Ghorabaee, M. K., Turskis, Z., 2017. An Extension of The EDAS Method Based on The Use of Interval Grey Numbers. Studies in Informatics and Control, **26**(1), pp. 5 – 12.

[21] Mathew, M., Sahu, S., 2018. Comparison of New Multi-Criteria Decision Making Methods for Material Handling Equipment Selection. Management Science Letters, **8**(3), pp. 139 – 150.

[22] Chatterjee, P., Banerjee, A., Mondal, S., Boral, S., Chakraborty, S., 2018. Development of a Hybrid Meta-Model for Material Selection Using Design of Experiments and EDAS Method. Engineering Transactions, pp. 1 – 21.

[23] Caloglu Buyukselcuk, E., 2020. Cold Chain Logistics Firm Selection by Using AHP-VIKOR Integrated Method and a Case Study in Food Industry. pp. 403–415. https://doi.org/10.1007/978-3-030-31343-2_35.

[24] Hussain, S., Mandal, U., 2016. Entropy Based MCDM Approach for Selection of Material, National Level Conference on Engineering Problems and Application of Mathematics.

[25] Ersoy, N., 2018. Entropy Tabanlı Bütünleşik ÇKKV Yaklaşımı ile Kuramsal Sürdürülebilirlik Performans Ölçümü. Ege Akademik Bakış, **18**(3), pp. 367 – 385.

[26] Ocampo, L., Deiparine, C.B., Go, A.L., 2020. Mapping Strategy to Best Practices for Sustainable Food Manufacturing Using Fuzzy DEMATEL-ANP-TOPSIS. Eng. Manag. J., **32**, pp. 130–150. https://doi.org/10.1080/10429247.2020.1733379.

[27] Kaviani, M.A., Karbassi Yazdi, A., Ocampo, L., Kusi-Sarpong, S., 2019. An Integrated Grey-Based Multi-Criteria Decision-Making Approach for Supplier Evaluation and Selection in The Oil and Gas Industry. Kybernetes, **49**, pp. 406–441. https://doi.org/10.1108/K-05-2018-0265.

[28] Yazdani, M., Chatterjee, P., Pamucar, D., Abad, M.D., 2019. A Risk-Based Integrated Decision-Making Model for Green Supplier Selection. Kybernetes, **49**, pp. 1229–1252. https://doi.org/10.1108/K-09-2018-0509.

[29] Galankashi, M.R., Helmi, S.A., Hashemzahi, P., 2016. Supplier Selection in Automobile Industry: A Mixed Balanced Scorecard–Fuzzy AHP Approach. Alexandria Engineering Journal, **55**, pp. 93–100. https://doi.org/10.1016/j.aej.2016.01.005.

[30] Liu, J.Y., Shiue, W., Chen, F.H., Huang, A.T., 2019. A Multiple Attribute Decision Making Approach in Evaluating Employee Care Strategies of Corporate Social Responsibility. Manag. Decis. **57**, pp. 349–371. https://doi.org/10.1108/MD-03-2018-0230.

[31] Prakash, C., Barua, M.K., 2016. A Combined MCDM Approach for Evaluation and Selection of Third-Party Reverse Logistics Partner for Indian Electronics Industry. Sustain. Prod. Consum., **7**, pp. 66–78. https://doi.org/10.1016/j.spc.2016.04.001.

[32] Mohammed, A., Harris, I., Dukyil, A., 2019. A Trasilient Decision Making Tool for Vendor Selection: A Hybrid-MCDM Algorithm. Manag. Decis., **57**, pp. 372–395. https://doi.org/10.1108/MD-04-2018-0478.

[33] Dweiri, F., Kumar, S., Khan, S.A., Jain, V., 2016. Designing an Integrated AHP Based Decision Support System for Supplier Selection in Automotive Industry. Expert Syst. Appl., **62**, pp. 273–283. https://doi.org/10.1016/j.eswa.2016.06.030.

[34] Merdivenci, F., Oğuz, S., 2020. Entropi Tabanlı EDAS Yöntemi ile Personel Seçimi: Lojistik Sektöründe Bir Uygulama. Gümüşhane Üniversitesi

Sosyal Bilimler Enstitüsü Elektronik Dergisi, **11**(3), pp. 615 – 624.

[35] Özaydın, G., Karakul, A., 2021. Entropi Tabanlı MAUT, SAW ve EDAS Yöntemleri ile Finansal Performans Değerlendirmesi. Süleyman Demirel Üniversitesi İktisadi ve İdari Bilimler Fakültesi Dergisi, **26**(1), pp. 13 – 29.

[36] Ali, T., Ma, H., Nahian, A. J., 2019. An Analysis of The Renewable Energy Technology Selection in The Southern Region of Bangladesh Using a Hybrid Multi-Criteria Decision Making (MCDM) Method. International Journal of Renewable Energy Research, **9**(4), pp. 1838 – 1848.

[37] Voelcker, J., 2021. EVs explained: Battery capacity, gross versus net. Retrieved from https://www.caranddriver.com/features/a36051980/evs-explained-battery-capacity-gross-versus-net/.

[38] Erhan, K., Ayaz, M., Özdemir, E., 2013. Elektrikli Araç Şarj İstasyonlarının Güç Kalitesi Üzerine Etkileri. Akıllı Şebekeler ve Türkiye Elektrik Şebekesinin Geleceği Sempozyumu, Ankara.

[39] Gasbaoui, B., Chaker, A., Laoufi, A., Allaoua, B., Nasri, A., 2011. The Efficiency of Direct Torque Control for Electric Vehicle Behaviour Improvement. Serbian Journal of Electrical Engineering, **8**(2), pp. 127 – 146.

[40] Sanguesa, J. A., Torres-Sanz, V., Garrido, P., Martinez, F. J., Marquez-Barja, J., 2021. A Review on Electric Vehicles: Technologies and Challenges. Smart Cities, **4**(1), pp. 372 – 404.

[41] Grunditz, E. A., Thiringer, T., 2018. Electric Vehicle Acceleration Performance and Motor Drive Cycle Energy Efficiency Trade-Off. XIII. International Conference on Electrical Machines, pp. 717 – 723.

[42] Yüksekyıldız, E., 2021. Entropi ve EATWOS Yöntemleri ile Türkiye Konteyner Limanlarının Verimlilik Analizi. Verimlilik Dergisi, **2**, pp. 3 – 24.

[43] Wu, J., Sun, J., Liang, L., Zha, Y., 2011. Determination of Weights for Ultimate Cross Efficiency Using Shannon Entropy. Expert Systems with Applications, **38**(5), pp. 5162 – 5165.

[44] Yüksekyıldız, E., 2020. Türkiye Kruvaziyer Limanlarının Performans Değerlendirmesi. European Journal of Science and Technology, **3**, pp. 607 – 615.

[45] Keshavarz Ghorabaee, M., Zavadskas, E.K., Olfat, L., Turskis, Z., 2015. Multi-Criteria Inventory Classification Using a New Method of Evaluation Based on Distance From Average Solution (EDAS). Informatica, **26**, pp. 435–451.

[46] Ulutaş, A., 2017, EDAS Yöntemi Kullanılarak Bir Tekstil Atölyesi için Dikiş Makinesi Seçimi. İşletme Araştırmaları Dergisi, **9**(2), pp. 169-183.

[47] Gabbatiss, J., 2019. Electric Vehicles Already Able to Cut Greenhouse Gas Emissions by Half. The Independent, ESI Media.

[48] Nealer, R., Reichmuth, D., Anair, D., 2015. Cleaner Cars from Cradle to Grave: How Electric Cars Beat Gasoline Cars on Lifetime Global Warming Emissions. Cambridge: Union of Concerned Scientists.

[49] Dunning, B., 2019. No, Electric Cars Don't Pollute More. Retrieved from https://skeptoid.com/episodes/4687?fbclid=IwAR3TjNmLH9rIft2uJkLeS7ksXzyvR8XOklutpBJQLFSqGOu2AZvBbg0MUtA.


KOCAELI UNIVERSITY
1992